A NAWDEX case study: Water vapor transport in atmospheric rivers and quantifying hand over of moisture between extratropical cyclones

Petter Ekrem

Supervisor: Harald Sodemann

September 25, 2020

University of Bergen
Faculty of Mathematics and Natural Sciences
Geophysical Institute

Contents

Abstract

Meridional water vapor transport occurs predominantly within the warm sector of extratropical cyclones. The warm sector is seperated by the cyclone's warm front ahead, and the cold front behind. In this region the warm conveyor belt or the atmospheric river reside. Little is known about the joint water vapor transport of multiple extratropical cyclones and their sequential interaction. This thesis attempts to identify if, and quantify how much water vapor left behind in the atmosphere by an extratropical cyclone, is incorporated into the airflow of the successive cyclone. The water vapor associated with the cyclone's center and its frontal structure have been separated to investigate which parts of the cyclone contributes the most to the process of "handover" of water vapor. The atmospheric model, COSMO-tag that is equipped with a water vapor tagging implementation, is used to identify the water vapor sources associated with the respective cyclones. Comparisons of observations gathered by dropsondes during the NAWDEX field campaign and model results show an over all good agreement in resolving the water vapor signature of atmospheric rivers. Model results indicate that substantial amounts of water vapor are handed over from one cyclone to another. Contributions of 10% to the total amount of moisture close to the cyclone's center is attributed to the handover process. Another remarkable result is the handover of moisture from atmospheric rivers into the cyclone's airflow and their association with precipitation contributions near the cyclone's center.

Acknowledgements

First of all I would like to thank my supervisor, Harald Sodemann for guiding me through the process of writing a MSc thesis in a time of remote communication and being stuck in home office, aswell as helping me through the frustration of getting the model to run properly.

I am also grateful for the NAWDEX team for inviting me to attend the workshop in Toulouse, France in March 2019. It's a great privilege for a master student to be a part of such a large international research team.

A huge thanks goes out to my main squad at GFI. All the laughs and way too long lunch breaks made the 5 years at GFI go by in a blink of an eye.

Finally, I would like to thank my parents for supporting me in my lifelong dream of becoming a meteorologist.

Chapter 1

Introduction

1.1 Introduction

Extratropical cyclones are the main contributors to precipitation in the North Atlantic and Northern Europe. Precipitation associated with cyclones account for 70-80 % of total precipitation in these regions (Hawcroft et al., 2012).The process responsible for precipitation in and from cyclones, is the warm conveyor belt (WCB) air flow. It is a region behind the cyclone's warm front, where moist air ascends, while being transported poleward (Harrold, 1972), thus generating precipitation.

The processes concerning how these cyclones transport and distribute moisture during their development phases, are fundamental to describe the intensity and amount of precipitation occurring. The process accountable for the largest amount of moisture transport in the atmosphere are termed Atmospheric Rivers (ARs) (Zhu and Newell, 1998). ARs are defined by a large flux of water vapor, and large values of vertically integrated water vapour, in narrow bands stretching across many degrees of latitude (e.g subtropics to midlatitudes). The large majority of meridional moisture transport in midlatitudes comes from ARs, even though they cover less than 10 % of the area of the Earth (Zhu and Newell, 1998). In a study by Sodemann and Stohl (2013), it was shown that individual cyclones were responsible for the formation and maintenance of ARs, and that the cyclone's WCB fed of the moisture from the AR, simultaneously as feeding it moisture that had accumulated behind the cyclone's cold front. However, very long ARs require more than one cyclone to be maintained, before the moisture is released as precipitation. This explains why there should be a distinction between the ARs and the classical WCB, since both phenomenon transport moisture in a similar manner, and are closely related. The WCB is a part of one individual cyclone, and the ARs can under right circumstances persist through multiple cyclones in succession and is therefore not necessary a part of one individual cyclone. Still, there is a lack of understanding in the process describing how the moisture from the ARs are handed over to a passing cyclone.

Since cyclones contribute 70-80 % to the total precipitation reaching Europe, it is important to address mechanisms that can alter the trajectories and the magnitude

of the cyclones. An important mechanism is the planetary wave-like behaviour of the tropopause jet stream. Thorncroft et al. (1993) proposed that depending on the state of this wave, it could alter the life cycle of the cyclones. They termed this Life Cycle 1 (LC1), when the jet had thinner wave troughs and a pronounced meridional direction, and Life Cycle 2(LC2) for when the jet had broader wave troughs and a pronounced zonally direction. During LC1 the general picture is more, but smaller cyclones, while LC2 indicates fewer, larger cyclones. One such LC1 situation investigated by Stohl et al. (2008) found that two successive cyclones, where the latter cyclone fed of the moisture from the first, contributed to extreme precipitation and flooding in south western Norway. This suggests that during LC1, there is a more pronounced meridional moisture transport in the AR. A schematic visualization of the patterns for the cyclones and ARs during LC1 and LC2 is given in figure 1.1.

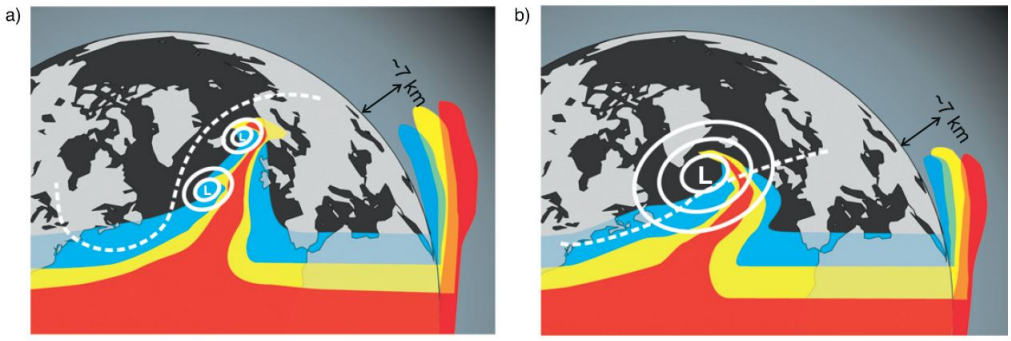

Figure 1.1: Schematic of a) LC1 and more pronounced meridional moisture transport in AR, b) LC2 and more pronounced zonal moisture transport in AR. The colored areas show vertical distribution of water vapor tracers. (Sodemann and Stohl, 2013)

1.2 Research aim

In this thesis I will be investigating a case resembling an anticyclonic LC1. A synoptic weather description can be found in section 4.2. I will be focusing on identifying and quantifying the moisture handover from one extratropical cyclone to other extratropical cyclones passing in succession and identifying if this handover is occuring multiple times from the same source of water vapor. Additionally I will be investigating the AR's contribution to the handover process. During this time period multiple cyclones and ARs form in a relatively short time and it is therefore reasonable to assume that the same source of water vapor can be present in different weather systems at different times. To simulate and investigate this phenomenon, the regional numerical weather prediction (NWP) model, COSMO will be used. This model is equipped with a tagging feature that makes it possible to track certain bodies of water vapor in the the model simulation. This is explained further in section 3.5. This also makes it possible to investigate the moisture origin of water vapor present in the domain and in the different weather systems. The model results

will be compared to observations from dropsondes measurements obtained during the North Atlantic Waveguide and Downstream Impact Experiment (NAWDEX) field campaign of 2016 aswell as the ERA-5 reanalysis data from ECMWF (European center for medium range weather forecasting) to validate the accuracy of the model.

Chapter 2

Theory and Background

2.1 Atmospheric river characteristics and identification

Newell et al. (1992) discovered a filementary structure when investigating global tropospheric water vapor fluxes. These filaments were many times longer (about 2000km) than their widths (about 300-500km) and stretched over several degrees of latitude or longitude. They called these filaments tropospheric rivers, as some of these flow patterns had similar water fluxes as terrestrial rivers like the Amazon. However the scientific term was later changed to "Atmospheric River" by Zhu and Newell (1998). The strong fluxes occur due to strong low level winds, also known as low level jets. On average, 4-5 of these rivers are typically present at all times in the northern hemisphere and they occur in the WCB of extratropical cyclones. However ARs have been identified and associated with tropical cyclones (Cordeira et al., 2013) and tropical cyclones that underwent extratropical transition (Stohl et al., 2008). Over 90% of all vertically integrated moisture transport in the midlatitudes occur in these narrow bands even though they cover less than 10% of the Earth's surface (Zhu and Newell, 1998), and they therefore play an important role in the atmospheric water cycle.

According to Gimeno et al. (2014), there are generally two approaches to detect ARs;

1. Looking at integrated water vapor(IWV $[mm]$) from satellite measurements, or by applying a threshold to IWV in reanalysis data where areas with greater IWV than 20 mm are identified.

2. Calulating integrated water vapor transport (IVT $[kgm^{-1}s^{-1}]$) from reanalysis data and applying a threshold to IVT where areas with values $> 250\ kgm^{-1}s^{-1}$ between 1000hPa and 300hPa are identified.

When these criteria are fulfilled to adjacent grid cells equivalent of a length of 2000km and more narrow than 1000km, an AR is identified. Because of the relatively short research period for this thesis and ARs being a visually striking phenomenon, the ARs were identified manually by looking at ERA5 reanalysis data of total column water vapor (TCWV) and applying a $20kgm^{-2}$ threshold value, and the

identification method therefore resembles method 1. Even though TCWV and IWV have different units, they represent the same amount of water vapor. IWV is the depth the fluid would occupy in a square meter if the water vapor in the atmospheric column would condense. TCWV is the total weight of the water vapor in the atmospheric column. For example $20kgm^{-2} <=> 20mm$.

Moisture sources refer to the identification of different bodies of water vapor that make up the total moisture of a portion of the atmosphere. This could include more local sources like sea surface evaporation, or evapotranspiration from land, or more remote sources from the subtropics or tropics. The moisture sources in an AR are typically from local moisture from sea surface evaporation and moisture convergence from a cold front that sweeps up evaporated moisture and feeds the AR (Dacre et al. (2015),Sodemann and Stohl (2013)), or moisture from the tropics/subtropics that has been transported poleward by the cyclone's air flow. However, there is some disagreement in the literature concerning which of these moisture sources have the largest contribution to the water vapor amount in an AR. Thus there is also disagreement in the appropriateness of the term "Atmospheric river", since the term "river" is unanimous with long distance water transport. In the studies by Sodemann and Stohl (2013) and Stohl et al. (2008) water vapor sources in precipitation falling over southern Norway were investigated. They found considerable amounts of water vapor contributions from subtropical regions in precipitation falling when an AR was present over southern Norway. Dacre et al. (2015) takes the view that evaporation from the sea surface behind the cyclones cold front is the largest contributor of moisture to the AR and that moisture convergence into the system is negligible. Thus they claim that as the cold front moves closer to the warm front, making the region between them more narrow, the local moisture convergence along the cold front creates the AR, i.e. the AR is the "footprint" of where the cyclone has been located.
To investigate and identify the moisture sources of water vapor in extratropical cyclones in this case study, I have separated the water vapor associated with close proximity to the cyclone centers and the water vapor associated with the cyclones frontal structure. Mapping out the water vapor sources for the different regions will give further insight in which water vapor source is contributing the most to the respective region of the cyclone, be it cyclone center or the cyclone's frontal structure. Results from this analysis can be found in section 5.3.

2.2 Atmospheric rivers and warm conveyor belts

Both ARs and WCBs are similar processes that transport considerable amounts of atmospheric water vapor and both are associated with cyclones. But under certain circumstances the distinction becomes more clear. When investigating a case resembling an anticyclonic LC1, Sodemann and Stohl (2013) found that ARs outlived individual cyclones, and that subsequent passing cyclones fed of the moisture from the AR and feeding their WCB. Simultaneously the cyclones fed moisture to the AR that had accumulated ahead of the cyclone's cold front. This indicates that there is a distinction between the AR and the WCB when the AR persists

long enough for it to "interact" with multiple cyclones, because a WCB is a part of the warm sector of an indivdual cyclone. The distinction between ARs and WCBs during a cyclonic LC2 is more unclear, and the processes seem to be more identical. Another distinction between the two processes are that ARs does not have the characteristic strong vertical ascent that is associated with WCB (Sodemann and Stohl, 2013).

There are generally two numerical methods used to investigate moisture origin or water vapor source contributions; The Eulerian approach, using moisture tracers and water vapor tagging, which is used in this thesis. Or an Lagrangian approach, using humidity variations on backward trajectories (Winschall et al., 2014). The Lagrangian approach mostly concern the short term difference between evaporation and precipitation, that an atmospheric particle are subject to during the model simulation. Using backwards trajectories reveals when and which of the two processes were dominant. This method is less computational heavy and more suitable for climate science applications (Winschall et al., 2014). One caveat of the Lagrangian method is when this humidity difference becomes near zero. This could indicate that little to no evaporation or precipitation is occuring, or it could indicate that both processes are equally contributing.
The concept of water vapor tagging in the Eulerian approach consists of releasing water vapor tracers from predefined domains/boxes in the model domain. When water vapor enters the domain through the chosen boundary it is tagged by the model. This makes it possible to track and quantify the water vapor source terms that is present in the domain. This approach is more elaborate than the Lagrangian approach, since it requires predefined sources i.e lateral boundaries or regional sub-domains. This approach is computational heavy and best used for case studies (Winschall et al., 2014). However Sodemann and Stohl (2013) applied this method for an entire month of run time. They made attempts of quantifying the fraction of remote and local moisture contributions of precipitation falling over south western Norway when an AR was present. In that study they released moisture tracers in bands at every 10^o latitude. The tracers were released when evaporation was identified by the model and they were then incorporated in the atmosphere's air flow. They found that under AR events the subtropical moisture sources in precipitation for south western Norway increased by a factor of 10-20, compared to non AR event. Simultaneously more local contributions decreased substantially.

Comparison between the two different approaches for the same case study were made by Winschall et al. (2014). They investigated the moisture sources for an extreme precipitation event in eastern Europe in 2010 that was associated with a cyclone that developed over northern Africa. Both methods agreed that moisture from the North Atlantic and local evapotranspiration were the dominant source terms that contributed to the rain event. However, the quantified amounts from the different sources differed from the two methods.

In this thesis, the Eulerian approach of water vapor tagging has been used since this makes it possible to predefine subdomains that release water vapor tracers, and for how long these tracers are released. Which means that water vapor tracers can

be released during selected events during a cyclone's lifespan, so one can monitor the amount of water vapor left behind in the atmosphere by a cyclone, and ultimately, the amount handed over from one cyclone to the other.

Chapter 3

Data and methods

3.1 Observations

The main focus of this thesis is the investigation of moisture origin in atmospheric rivers and extratropical cyclones and the handover of moisture between extratropical cyclones based on atmospheric model simulations. The observations obtained during the NAWDEX field campaign are therefore used to compare model results with observations as a form of model validation.

3.1.1 Dropsondes

A total of 289 dropsondes were released during the NAWDEX field campaign. However only, 63 of these coincide with the research period of this thesis. Of these 63 dropsondes only 31 were released in areas of interest. Four different research aircrafts were used to obtain observations during the NAWDEX field campaign; the DLR HALO,DLR Falcon, SAFIRE Falcon and FAAM BAe 146. All these aircrafts were equipped with dropsondes. However, in this thesis I will be using observations obtained from dropsondes released from the SAFIRE Falcon aircraft based on the targeted area for the respective flights. From the period 07-11.10.2016, the main targeted areas for the SAFIRE Falcon were ARs and WCB outflows, and dropsondes were released into these weather systems. An overview of dropsonde release time and location can be found in Table 3.1. Dropsondes released during flight RF07 were also in area of interest, but these were unfortunately not retrievable.

Plots of flightrack and dropsonde release location and dates for the individual flights RF10,RF11,RF12,RF13 and RF14 can be found in figure 3.1. The SAFIRE Falcon was also equipped with in-situ instruments for observations of pressure, temperature, wind, humidity, TAS aircraft position, heading, altitude (Schäfler et al., 2018). These observations are not used in the analysis because during flight the aircraft is situated above the weather systems of interest (i.e. ARs/WCB).

The dropsondes used were of the type "Vaisala RD94". The measurement frequency for humidity, temperature and pressure is 2 Hz and has a descent time of approximatly 8 minutes when released from 7.5 km (Vaisala RD94 manual). This measurement

frequency results in thousands of data points in a single vertical profile and has therefore been interpolated to represent one value per 1 hPa from 300 hPa to 1000 hPa i.e 700 data points. The same has been done to model results for intercomparison between the model results and the observations.

The dropsonde data have been used to compare vertical crossections of mixing ratio with vertical crossections of specific humidity from COSMO model results in the corresponding dropsonde locations. The comparison is done both for the coarse (deg=0.5) and the fine resolution (deg=0.1) runs. One exception is the dropsondes released during flight RF12 for the 9th of October. The aircraft made four crossections of the frontal area and moisture associated with the remnants of an extratropical cyclone (Cyclone 3, Figure 4.2 e). Pairs of dropsondes were released during two of the crossections made (see figure 3.1), thus the data gathered for the respective dropsondes will be compared with vertical profiles from the COSMO model results.

Table 3.1: Overview of dropsondes released from the research aircraft SAFIRE FALCON from the period 07-11.10.2016 during the NAWDEX field campaign.

Flight name	Dropsonde name	Date	Time (UTC)	Lon (°E)	(°N)	Note
RF10	D1(Red)	07.10.2016	14:06	-25.09	59.35	
RF10	D2(Magenta)	07.10.2016	14:11	-24.83	59.91	
RF10	D3(Cyan)	07.10.2016	14:16	-24.57	60.49	
RF10	D4(Blue)	07.10.2016	14:21	-24.28	61.10	
RF10	D5(Green)	07.10.2016	14:26	-23.95	61.71	
RF10	D6(Black)	07.10.2016	14:30	-23.70	62.19	
RF10	D7(Yellow)	07.10.2016	14:35	-23.41	62.71	
RF11	D1(Red)	09.10.2016	11:15	-17.09	61.62	
RF11	D2(Magenta)	09.10.2016	11:22	-15.43	61.60	
RF11	D3(Cyan)	09.10.2016	11:29	-13.89	61.58	
RF11	D4(Blue)	09.10.2016	11:36	-12.22	61.53	
RF12	D1(Red)	09.10.2016	17:55	-15.72	61.53	
RF12	D2(Magenta)	09.10.2016	18:04	-13.71	61.52	
RF12	D3(Cyan)	09.10.2016	19:16	-12.23	63.37	
RF12	D4(Blue)	09.10.2016	19:23	-14.23	63.56	
RF13	D1(Red)	10.10.2016	11:39	-3.99	62.62	
RF13	D2(Magenta)	10.10.2016	11:46	-5.55	62.73	
RF13	D3(Cyan)	10.10.2016	NaN	NaN	NaN	Instrument Error
RF13	D4(Blue)	10.10.2016	11:53	-7.04	62.93	
RF13	D5Green)	10.10.2016	11:59	-7.43	62.97	Instrument Error
RF13	D6(Black)	10.10.2016	12:06	-10.10	63.29	
RF13	D7(Yellow)	10.10.2016	12:13	-11.50	63.23	
RF14	D1(Red)	11.10.2016	17:18	-27.00	61.55	
RF14	D2(Magenta)	11.10.2016	17:26	-24.96	61.57	
RF14	D3(Cyan)	11.10.2016	17:34	-22.79	61.57	
RF14	D4(Blue)	11.10.2016	17:43	-20.57	61.54	

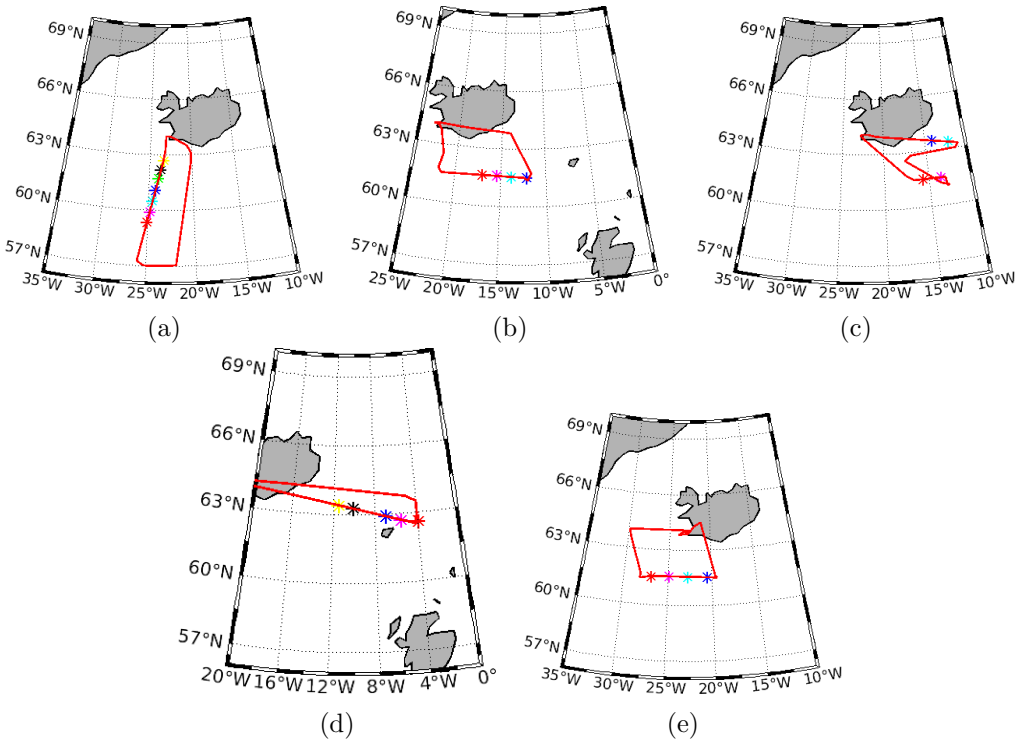

Figure 3.1: Flight track (red line) and dropsonde locations (colored (*) markers) released from the SAFIRE Falcon aircraft during NAWDEX from the flights a) RF10, b) RF11 c) RF12, d) RF13, e) RF14. See Table 3.1 for dropsonde release time and coordinates

3.2 ERA5-Reanalysis data

The ERA5 reanalysis data set is an publicly open data set that provides hourly estimates for atmospheric, land and oceanic variables, such as temperature, pressure, specific humidity. It has a resolution of 30 km grid cells and resolves the atmosphere in 137 levels. The model IFS model cycle year is Cy41r2 the data assimilation method used is a 12 hour 4D-var ensemble (Hersbach et al., 2020). The ERA-5 data set is applied to the preprocessing program INT2LM and ultimately used as input for the COSMO model simulations. The data analyzed for section 4.2, uses the interpolated version of the ERA-5 reanalysis data set that has 37 pressure levels and a temporal resolution of 3 hours. Individual plots of numerous different atmospheric variables have been analyzed to find an atmospheric condition that coincides with the NAWDEX field campaign and that is the most suitable for the thesis's main research question. The main variables investigated are TCWV and MSLP, since these give a striking visual component and makes identifying ARs and cyclones relatively simple.

3.3 AR detection

Due to the relatively short research period investigated in this thesis, the ARs were manually identified by applying a 20 kgm^{-2} threshold to the ERA-5 dataset from ECMWF. This method was used by Neiman et al. (2008), but the length and width threshold have not been applied here. Section 4.2 discusses the synoptic weather situation during the research period and the ARs are identified and discussed there.

3.4 Atmospheric model

3.4.1 INT2LM Preprocessing

The preprocessing program "Interpolation to local model "(INT2LM) is used to interpolate the boundary data from the ERA-5 reanalysis data set to the desired grid and resolution used for the COSMO model simulations. INT2LM also interpolates data in the vertical model layers. In this application the INT2LM program interpolates the ERA-5 data from 137 vertical layers down to 40 vertical layers. The data produced by INT2LM is used as input boundary data for the COSMO model simulations and it is therefore necessary to run the INT2LM program in advance. The temporal resolution used in this application is 6 hours, thus it creates boundary input data for the COSMO model at 6 hour intervals. The detailed INT2LM setup can be found in the appendix A.1.

3.4.2 COSMO Model

The consortium for small scale modelling (COSMO) model is a non-hydrostatic high resolution regional atmospheric prediction model. It has been designed for both scientific applications like to simulate mesoscale deep moist convection processes, and for operational NWP. To run the model for NWP or for case study purposes, it requires interpolation and boundary conditions from a host model. In this case the host model is ERA-5 reanalysis data from ECMWF. To create this boundary data, the interpolation program INT2LM is used. This program uses ERA-5 data as initial conditions and interpolates it to fit the grid of the COSMO model. Figure 3.2 shows the domain used in the COSMO model simulations. The southern part of the domain covers the end of the north Atlantic storm track, so that the extratropical cyclones could be sufficiently resolved in the model simulations. The reason for the domain being extended so far north is to resolve the full extent of some ARs present during the NAWDEX field campaign. See section 4.1 for a synoptic weather overview. The COSMO model uses second-order finite differences spatial discretisation and a Lorentz vertical staggered Arakawa C-grid grid structure. For time integration a two level, second-order timesplitting Runge Kutta scheme is used (Doms et al., 2013).

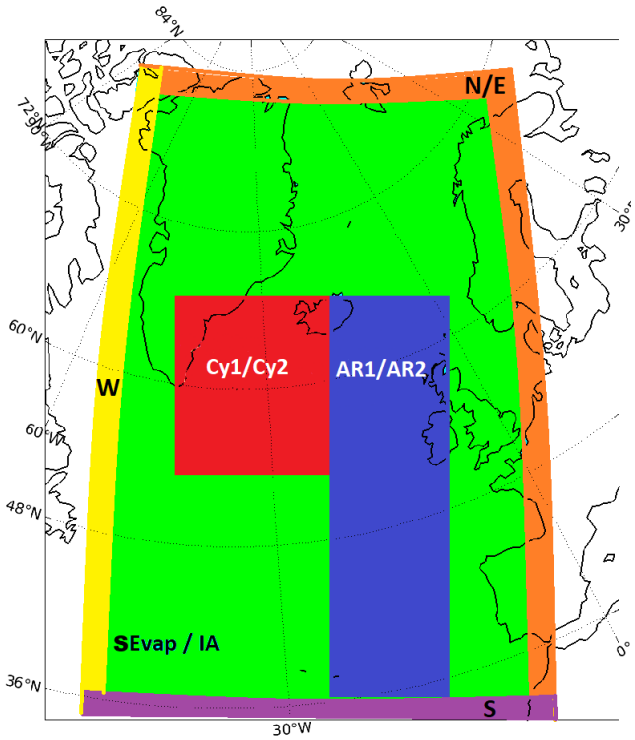

Figure 3.2: Schematic of model domain and subdomains/boxes used for tagging applications. Colored areas show moisture tracer sources from advection through North and Eastern (N/E), Southern (S), Western (W) boundaries. The boxes "Cy1/Cy2" and "AR1/AR2" represent two moisture sources each, activated at different lead times. Sources from evaporation (SEvap) and initial atmospheric tracers (IA) are released in the same area; Green color. Evapotranspiration tracers (LEvap) are released from land surfaces

3.5 Water vapor tagging

The COSMO model was equipped with a tagging implementation. This makes it possible to define regions within the model domain where atmospheric tracers are released. For example predefined lateral boundaries. When moisture is advected through one of these boundaries it is tagged by the model and is henceforth traceable to it's respective boundary. This makes it possible to identify different bodies of water vapor in different weather systems present in the model domain. And most importantly this approach makes it possible to quantify the amount of water vapor contributed from the different sources. This tagging implementation does not interfere with any model physics the air parcel undergoes during the simulation. This method has been previously used by Sodemann and Stohl (2013) and Winschall et al. (2014) to identify moisture origin in precipitation.

Additionally, water vapor released from evaporation is tagged continuously throughout the model simulation.Separate tagged variables are created from sea surface evaporation and evapotranspiration from land. This is defined separately from the COSMO

model simulation and is done using a program called "make_slab". This program uses the land fraction variable from COSMO model results and creates a file for the sea surface and land by treating land fraction values > 0.5 as land, and land fraction values < 0.5 as sea surface. These files are used as input in the COSMO model to detect and tag water vapor from evaporation and evapotranspiration from sea surface and land, respectively.

The moisture tagging only applies to the atmospheric part of the model. When the water vapor condenses and is turned into precipitation that reaches the surface, it is no longer tagged. However the precipitation itself is traceable to the respective boxes.

3.6 COSMO model setup and simulations

For this application four different lateral boundaries/boxes were defined in the; southern , western, eastern and northern end of the domain. The moisture that is advected into the model domain through these boxes will be given a respective tag. One exception has been made with the Northern boundary box. There is negligible contributions from this boundary so the Northern and the Eastern lateral boundaries are given one tag. These lateral boundaries cover a width of 4 grid points which means that the area covered depends on the resolution of the model run. An additional box was defined as an inner sub-domain that these 4 boundaries encompass. This represents the amount of water vapor present in the initial atmosphere. The moisture in the inner domain is not traceable since it represents moisture in the domain during the model initialisation, it is therefor only tagged during the initialisation stage after sufficient spin up (Tagged for 10 minutes after 3 hours of simulation time). The moisture entering through advection into the 4 other boxes are continuously tagged throughout the model simulation period.

To simulate and quantify the handover of water vapor between extratropical cyclones, four different boxes where defined. The boxes "Cy1/Cy2" was predefined in the area where the mature cyclones were situated. These boxes occupy the same area in the domain, but they are activated at different lead times during the simulation, resulting in two separate tagged variables. This is also the case for the "AR1/AR2" box. The "AR1/AR2" boxes was predefined in the approximate region where the WCB, the frontal structures and the ARs usually are occupying. The boxes "Cy1", "AR1" and "Cy2", "AR2" are activated in pairs and release tracers for 3 hours of simulation time from the time step of when the respective cyclone reaches it's deepest pressure. The tagged variables from these boxes act a "snapshot" of the total amount of water vapor in the respective cyclone system (Both cyclone center and frontal structure). An important thing to note is that even though the tracers are only released for 3 hours of simulation time, the tracers still remain in the atmosphere and is incorporated into the airflow of the model. A schematic of the

model domain and the different boxes that release water vapor tracers can be found in Figure 3.2.

The two main model runs conducted are named "run050" and "run010", representing the coarse and the fine resolution run, respectively. Run050 has 72x98 grid points and run010 has 360x490 grid points. Further details of the model runs can be found in table 3.2. Details concerning the tagging variables enabled as well as tracer initialization time can be found in Table 3.3.

Table 3.2: COSMO simulation details

Model run	Sim. Start	Sim. end	Run time	Res.	Nr. tagged variables
run050	01 Oct 00 UTC	11 Oct 00 UTC	240 h	0.5 deg	5
run010	01 Oct 00 UTC	12 Oct 00 UTC	264 h	0.1 deg	10

Results from the coarse resolution run, run050 has only been used in model validation in sections 5.1 and 5.2. Further analysis is based on results from the finer resolution run, run010.

Table 3.3: List of tagged variables and their respective box for run010. t_i is the timestamp in seconds of simulation for tagging initialization. t_e is the timestamp for when tagging is turned off for the simulation.

Variable name	Tagging box	t_i [s]	t_e [s]
TAG1	IA	10600	11200
TAG2	N/E	10600	950400
TAG3	W	10600	950400
TAG4	S	10600	950400
TAG5	Cy1	151200	162000
TAG6	AR1	151200	162000
TAG7	Cy2	378000	388800
TAG8	AR2	378000	388800
TAG9	SEvap	10600	950400
TAG10	LEvap	10600	950400

3.7 Model validation

3.7.1 Model accuracy

The statistical property root mean square error (RMSE) is used to measure model accuracy when predicting quantitative data. It is the standard deviation of the residual term; $residual = (f - o)$, in this case the model forecasted value minus the analysis value. It indicates how concentrated the data is around the "line of best fit", or in this case; how well the model represents the observations/reanalysis. It is a squared quantity and is therefore never negative regardless of model over or

underestimation. Because of the square root it has the benefit of maintaining the physical dimensions of the property. From Warner (2011) RMSE is defined as :

$$RMSE = \sqrt{\frac{1}{n}\sum_{i=1}^{n}(f-o)^2} \tag{3.1}$$

An additional statistical property used in model validation measuring is the mean error (ME), also called the bias. It indicates if the model favours values higher,lower or similar to the observations/analysis, depending on the sign of the bias value. If the bias is 0, the model forecasts identical values to observations of the variable. From Warner (2011) the bias is given by :

$$Bias = \frac{1}{n}\sum_{i=1}^{n}(f-o) = \overline{f} - \overline{o} \tag{3.2}$$

In this thesis these properties have been calculated for specific humidity at 850 hPa and used to compare the interpolated reanalysis from INT2LM and the forecasted results from the coarse resolution COSMO run050.

Chapter 4

Study Area

4.1 NAWDEX field campaign

During The NAWDEX field campaign, extensive ground and airborne measurements were made in the North Atlantic basin. Measurements were made concerning the diabatic processes controlling midlatitude weather. This was done to improve the prediction of the uncertainties occurring in numerical weather prediction (NWP) when forecasting the occurrence of extratropical cyclones (Schäfler et al., 2018). The field campaign took place on Iceland in September and October in 2016, where this period was divided into 15 different intensive observation periods (IOPs). In this thesis I will be using observations that were made during IOP 6,7 and 8. Observations were done using 4 different air crafts equipped with remote sensing and in-situ instruments as well as from dropsondes released during flight.

4.2 Synoptic weather situation

In this section I will give an overview of the weather situation, and the weather evolution for the North Atlantic for the period 01.10.2016 - 11.10.2016. I will give the weather overview based on plots made with the ERA-5 reanalysis data from ECMWF. Specifically looking at TCWV, VIWVD (Vertical integral of water vapor divergence), MSLP , temperature, wind speed and direction at 850 hPa and geopotential at 500 hPa. The briefest summary is; three cases of cyclone development and the presence of three different ARs. Some atmospheric rivers stretch as far as from the coast of Portugal all the way to the Svalbard archipelago.

On 01.10.2016 there is a developing cyclone in the mid Atlantic (50 N, 40 E) (Figure 4.1 a). This will be referred to as Cyclone A. As Cyclone A is further intensifying, reaching hurricane force winds (32,7 m/s) and moving northward, it is transporting large amounts of water vapour in its eastern flank. At approximately 02.10 18:00 UTC, cyclone A reaches its lowest pressure, with a wind field with hurricane force stretching from 40 - 55 ^{o}N. There is now an atmospheric river(AR1), in a spiraling shape, stretching from 35^{o}N to 63^{o}N, near the west coast of Iceland (Figure 4.1 b). As this cyclone dissipates during the course of the next 36 hours, there is a high pressure system developing over Scandinavia. The high pressure system remains

quasi-stationary over Scandinavia for the remainder of this entire period. This is creating a funnel for the atmospheric river left behind by Cyclone A, making the moisture transport much more meridionally pronounced(Figure 4.1 c). At 03.10 18:00 UTC there is a second cyclone (Cyclone B) developing near the same location where Cyclone A developed from (50^oN, 40^oE). Cyclone A is now dissipating and is located at the cape of Greenland, resulting in an upper level trough in geopotential in this region. At 04.10 03:00 UTC Cyclone 2 is developing and is located east of this upper level trough (Figure 4.1 d) shows the effect of this 9 hours later. Upper level trough/Geopotential is not shown). Due to the high baroclinicity, Cyclone B is expected to intensify rapidly and then generate the second AR (AR2). AR1 now stretches from the coast of Portugal to Jan Mayen island (70^oN) (Figure 4.1 d). The VIWVD shows that the northern part of AR 1 is moving north eastward, but large amounts of the moisture further upstream is now semi-stationary. Especially near south west coast of Ireland, where there is almost no signal in VIWVD. This makes it possible for AR2 to catch up with parts of AR1 and eventually merge together as one AR. In under 24 hours at 05.10 00:00 UTC, Cyclone B reaches its deepest (approximately 960 hPa). There are now two atmospheric rivers present in the north Atlantic (AR1 and AR2). AR1 now stretches from the coast of Portugal to the Svalbard archipelago. Cyclone B is now quasi-stationary east of the cape of Greenland. North of Newfoundland at 05.10 00:00 UTC there is a some moisture being advected eastward (Not nearly as much as there is in the ARs, but there is still a strong signal in VIWVD)and wind speeds in this region are relatively high, considering how far away it is from the cyclone in the North Atlantic. At 05.10 18:00 UTC AR1 and AR2 have merged together as one. One can see two ARs in Figure 4.1 e), AR1 near the western coast of Ireland and AR2 to the west of AR1. 24 hours later, in Figure 4.1 f), we see that AR1 and AR2 have merged and is head on with southern Iceland. While the two ARs have merged, the moisture that was located north of Newfoundland is now located west of Newfoundland.

At 06.10 06.00 UTC there is secondary cyclogenesis occurring at approx. 50^oN, 33^oW. Since this cyclone (cyclone C) is developing further north and in a relatively cold region, cyclone C does not generate the same water vapor flux as the two previous cyclones, and it does not intensify in the same way as the previous ones either, reaching its deepest at 990 hPa (Figure 4.1 g). Because the MSLP in cyclone C is not as deep as Cyclone A and B, the water vapor is no longer confined as much as in the previous cases and is spread more evenly. However the water vapor does seem to merge together with the AR from the previous cyclones at 07.10 15:00 UTC

The AR that is extending from the subtropics to Svalbard changes it's orientation from northwards at 06.10 12:00 UTC (Figure 4.1 f) to a north westward orientation during Cyclone C's development (Figure 4.2 a). Substantial amounts of water vapor from the AR is therefore situated in proximity to Cyclone C's center during it's early development. This AR was investigated with the SAFIRE Falcon aircraft during the NAWEX field campaign. At 08.10 12:00 UTC the remnants of the AR is shifting its orientation back to predominantly northward flow. Simultaneously the water vapor transport associated with cyclone C's WCB is oriented in a similar

northward direction. On the 09.10 12:00 UTC, Cyclone C has created a distinct frontal signature of water vapor just east of Iceland (Figure 4.2 c). This signature is also identified as an AR and was also investigate by the SAFIRE Falcon aircraft during the NAWDEX field campaign (section 5.2).

This synoptic overview can give qualitative information about the handover of moisture between the cyclones and the atmospheric rivers. The cyclones seem to maintain the existence of the ARs, and when these ARs merge and shift orientation into the cyclone centers, therefore it is reasonable to assume that there is an exchange of moisture from the ARs into the mature cyclone. While in this case it seems this handover of moisture is not intensifying the cyclones, it perhaps is extending the cyclones life time, leading to a relationship between the two processes, where the AR and the cyclone are maintaining each other at different development stages.

An overview of the weather situation for the entire period is shown in Figure 4.3 b). The diagram is fixed at 60^oN and shows TCWV and MSLP for 40^oW to 5^oE, and the time evolution on the y-axis.

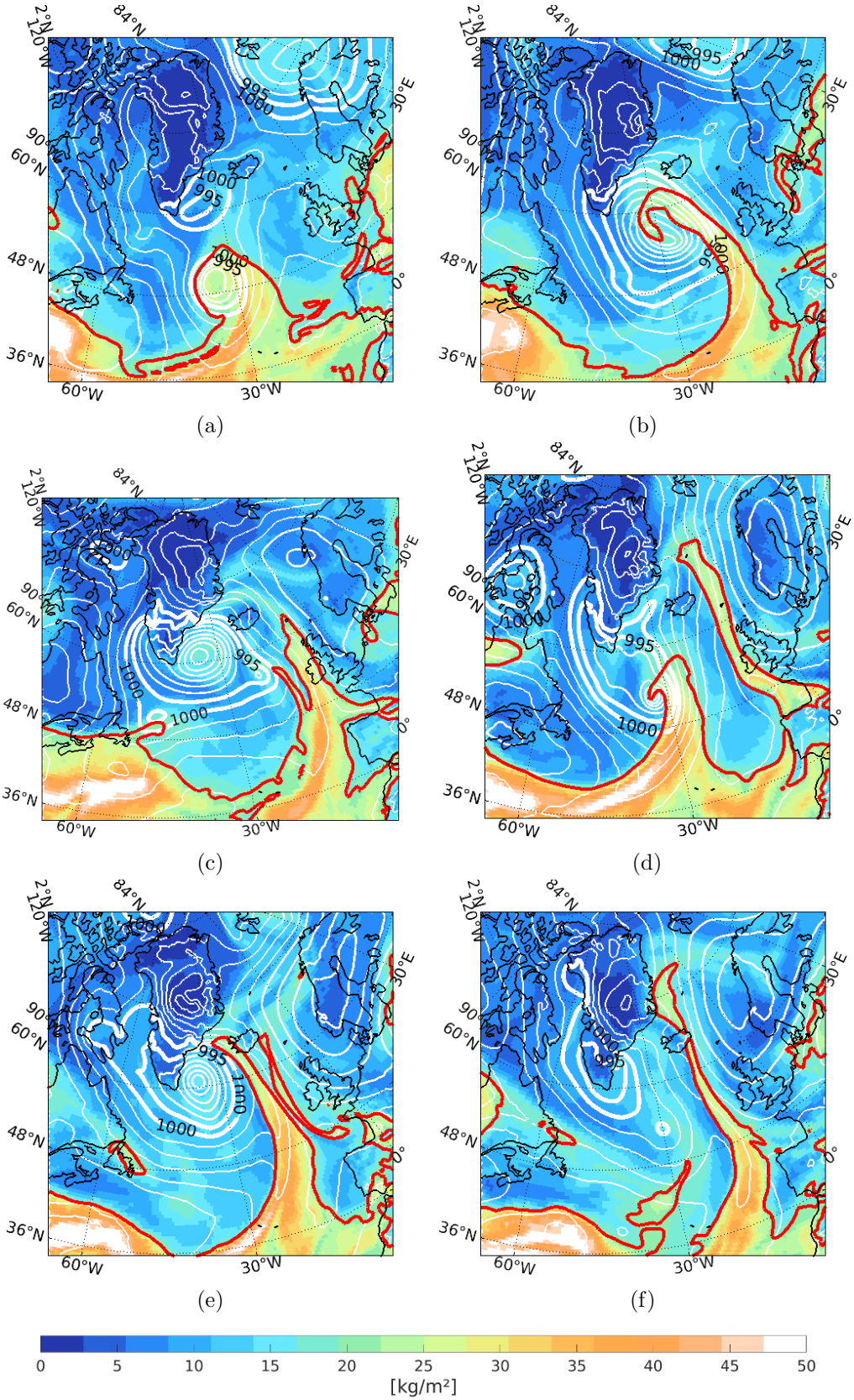

Figure 4.1: (a)-(g) shows total column water vapor (Shading; kgm^{-2}) and mean sea level pressure (White contours; 5 hPa intervals) from ERA5 reanalysis data for the North Atlantic for the period 01-06.10.2016 at 12:00 UTC. Two thicker white lines are shown, representing contour lines for 1000hPa and 995 hPa. The red contour line shows the $20kgm^{-2}$ AR threshold value.

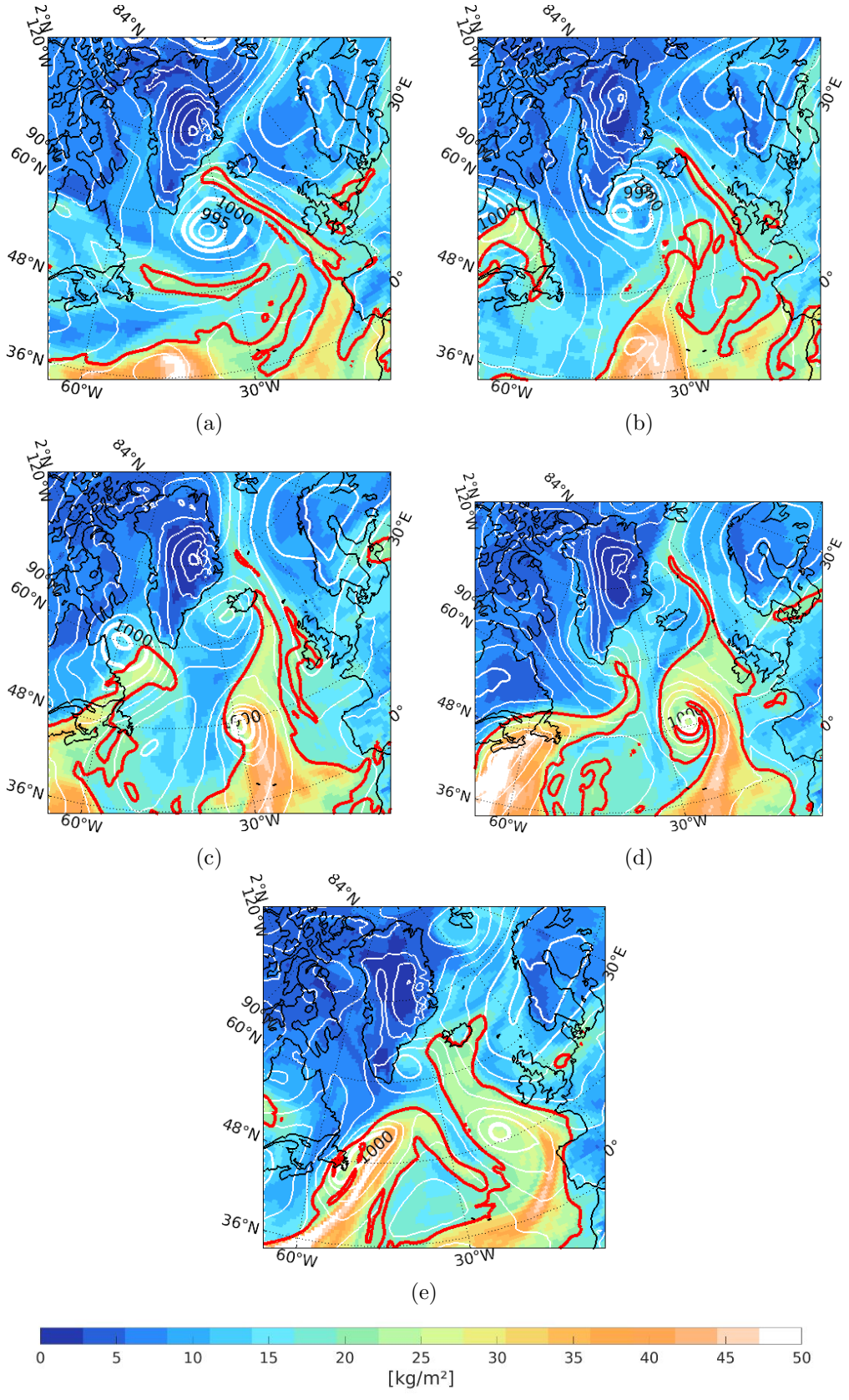

Figure 4.2: a)-e) same as Figure 4.1 but for the period 07-11.10.2016

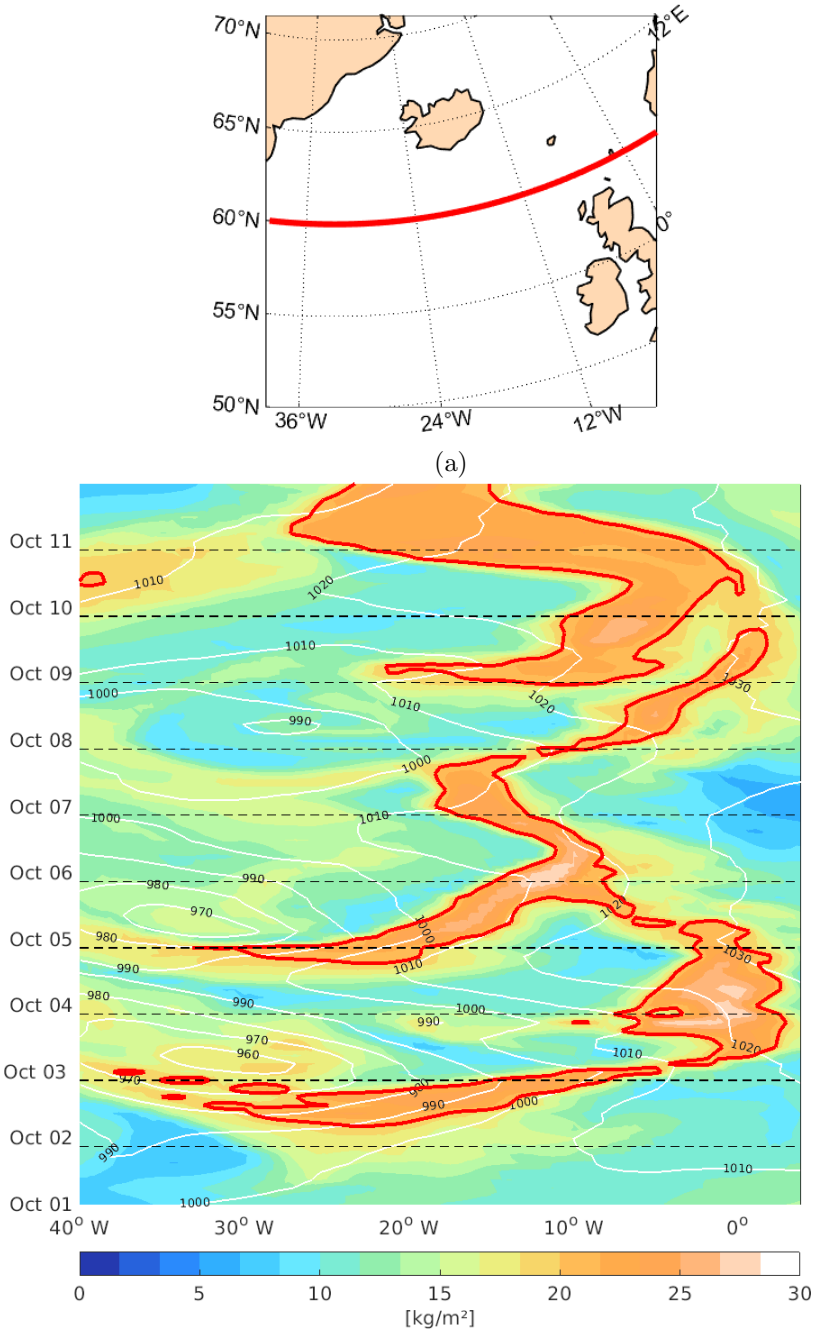

Figure 4.3: a) Map of a region of the North Atlantic. Iceland and parts of the UK are visible. The red line indicates at which latitude the Hovmöller diagram in b) is fixed. b) Hovmöller diagram for TCWV (Shading; $kg\ m^{-2}$) and MSLP (White contours; hPa;) from ERA-5 reanalysis, centered around 60^{o}N, for the period 01-11.10.2016. Red line highlightes the 20 $kg\ m^{-2}$ AR threshold. X-axis shows grid length in longitude. Dashed black lines indicate time intervals of +24 hours, ascending from the bottom of the figure. At October 5, 12:00 UTC we see the two ARs merging together

Chapter 5

Results

5.1 Model validation

Before one starts to apply model results, it is important to investigate if the model accurately represents actual events.In this section I will be presenting results from model validation of model run050. This analysis was done before any of the other model runs in Table 3.2 were conducted. This was done to ensure that the model domain extended far enough to resolve the weather systems of interest and that there was a clear separation between the atmospheric tracers advected in from the Southern and Western boundaries.

A common method of comparing quantitative data from model results and observations, or in this case reanalysis data is to calculate the bias and the RMSE. Figure 5.1a shows a timeseries of the bias for specific humidity at 850hPa for the period 01-09.10.2016. The bias fluctuates between positive (0.05 g/kg) and negative values (-0.05 g/kg) throughout the research period and has a mean value of 0.0185 g/kg. No clear trend in under/over-representation of moisture at this level can be identified. The magnitude of the bias is low compared to actual values of specific humidity at this level. For this case, typical values for specific humidity inside WCBs are around 8-12 g/kg.

The bias is calculated and averaged over a large area covering major parts of the eastern north Atlantic and large regional differences will therefore potentially be smoothed out. Larger differences in bias are identified by looking at the calculated bias at individual time steps. This difference is not averaged but it is a direct difference between COSMO model values and int2lm values for each grid point. Figure 5.2 shows this difference plotted together with MSLP from the COSMO model to give a relative position to the cyclone centers. On figure 5.2 c) south of Ireland where the first atmospheric river is located (not shown), there is an alternating pattern in the bias, from negative to positive values. The red and blue shadings in this region deviates approximately equally from zero, around -2 and +2 g/kg, indicating that the amount of water vapor is well represented by the model, but the position of the water vapor is not well resolved. This is a reoccurring pattern throughout the period in most of the very moist regions like in the eastern flanks of

the extratropical cyclones (Figure 5.2 e, g). The bias values for the entire domain (Figure 5.1a) are much lower than the ones found in each individual time steps. This supports the claim that the amount of water vapor present in the domain is well represented by the model.

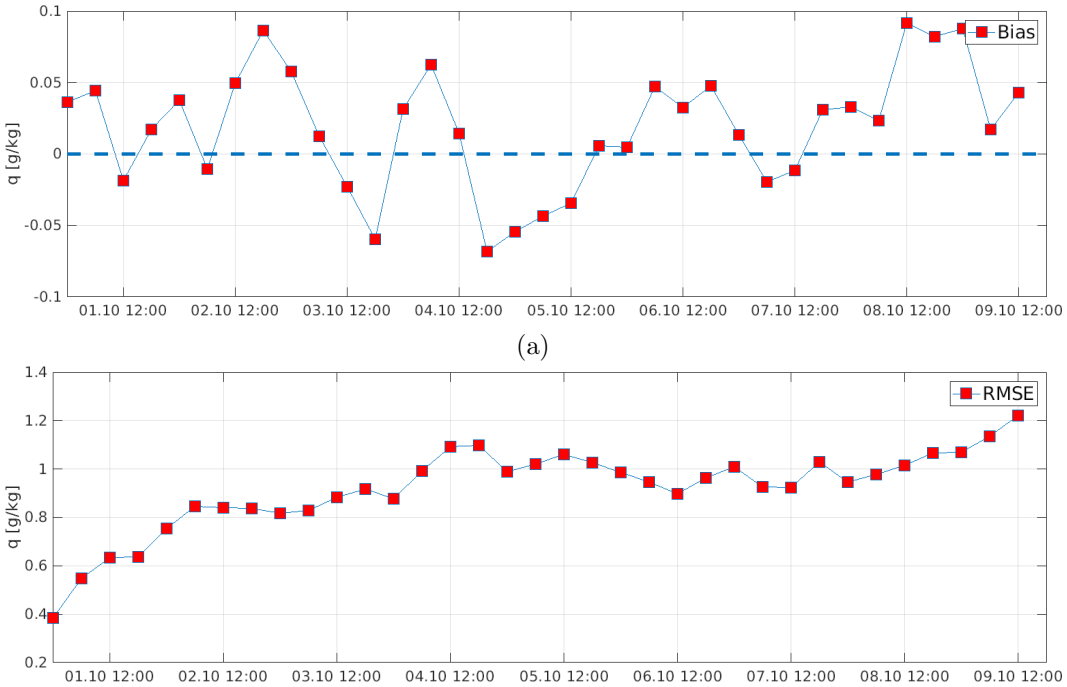

Figure 5.1: Time series of a) specific humidity bias at 850 hPa and b) RMSE for specific humidity[g/kg] at 850hPa between the COSMO(run050) model and int2lm(ERA5) for the period 01-09.10.2016. The bias and RMSE is calculated and averaged over the entire model domain for each time step. Red boxes shows calculated values while blue line shows interpolation between calculated values. X-axis show month/date/hour

Figure 5.1b shows the RMSE at 850 hPa calculated for the entire model domain and the period 01-09.10.2016. Since this is a squared quantity it is more sensitive to errors than the bias and it will therefor show larger values. It increases rapidly the first 24 hours of the simulation from initially $0.4 g/kg$ to 0.9 g/kg at 02.10.2016 12:00. Here it reaches somewhat of a plateau with small fluctuations throughout the period. As discussed with the bias, because of the large area this quantity is being averaged over, regional differences can be smoothed out. Figure 5.3 shows the RSE (root squared error) for the same time steps discussed for the bias. The figure also shows MSLP to give relative position to the cyclones. This is no longer a RMSE by definition because no averaging has been done in this calculation, only a direct squared difference between the COSMO model result and int2lm(ERA5). But it still shows how accurately the model represents actual events. The RSE has the largest values in the same regions as the bias (5.3 a)).

In Figure 5.3 c) there is a large black band in the middle of the domain. This

large error can be explained by the fact that there are two ARs present in this region at this time. The two ARs are in close proximity to each other since this is about 12 hours before they merge together as one AR. Since the model has some issues resolving the position of the moisture in the domain, it is unsurprising that the presence of two very moist regions will give a large signal in RSE.

Both the bias and the RMSE show large regional differences, especially in very moist regions near the extratropical cyclones, and in areas in close proximity to ARs. However the bias calculated over the entire domain have near zero values and is fluctuating between +0.05 and -0.05 g/kg. No clear trend can be identified from the bias either and the model is therefore neither over- nor underrepresenting moisture at this level. The regional differences bias (Figure 5.2) and the low domain total bias (Figure 5.1a) therefore indicates that the total amount of water vapor is well represented, but it has issues with the location of water vapor.
Similar results have been found by Wick et al. (2013), where they evaluated the forecasted water vapor signature of IWV in ARs with a NWP model. They found that the model could identify the presence of ARs and the water vapor signature were overall well represented independent of lead time. However, the position of the water vapor in said ARs, specifically landfalling ARs, were not sufficiently resolved compared to reanalysis.

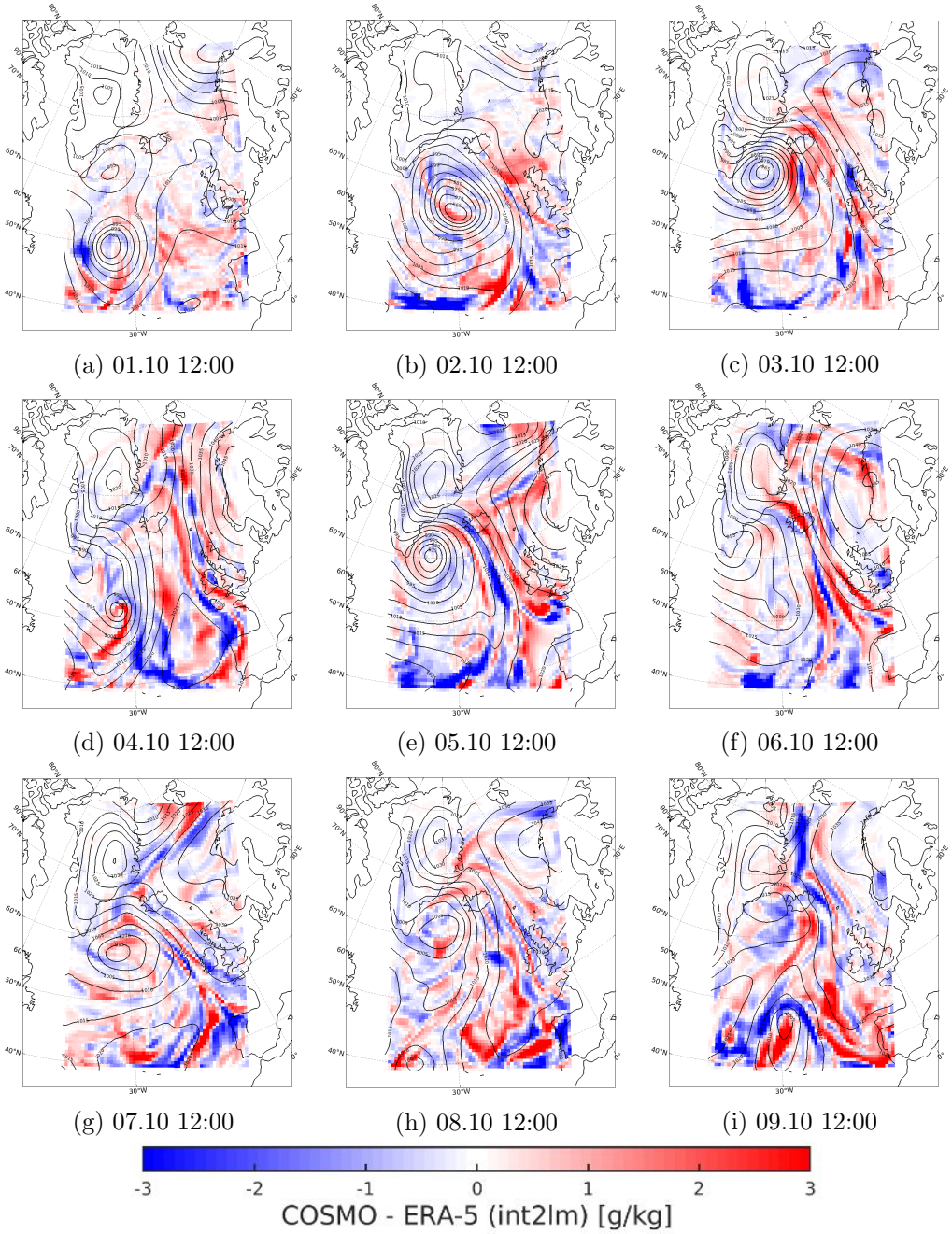

(a) 01.10 12:00 (b) 02.10 12:00 (c) 03.10 12:00

(d) 04.10 12:00 (e) 05.10 12:00 (f) 06.10 12:00

(g) 07.10 12:00 (h) 08.10 12:00 (i) 09.10 12:00

Figure 5.2: a)-i) Specific humidity bias at 850hPa(shading;g/kg) and MSLP from COSMO(black contours; hPa) for the period 01-09.10.2016

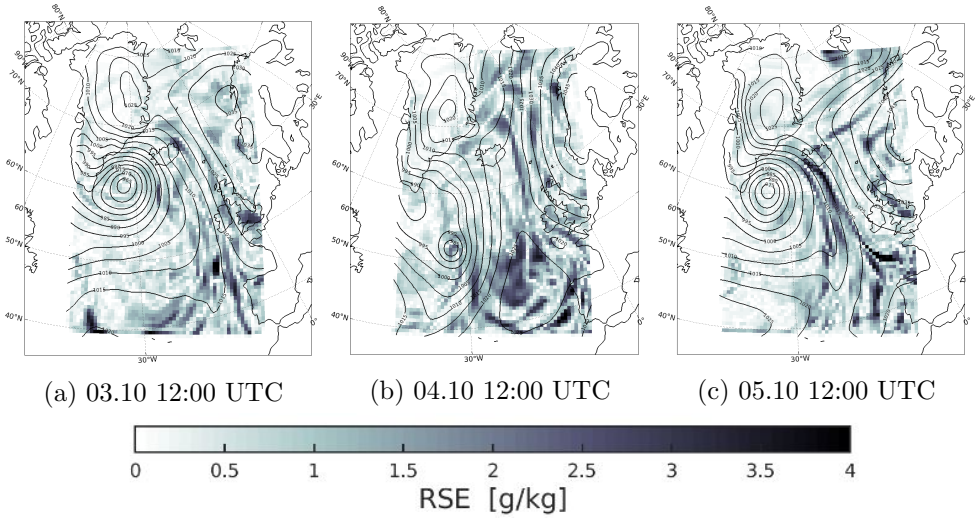

(a) 03.10 12:00 UTC (b) 04.10 12:00 UTC (c) 05.10 12:00 UTC

Figure 5.3: a)-c) RSE for specific humidity at 850hPa(shading;g/kg) and MSLP from COSMO(black contours;hPa) at a) 03.10.2016 12:00 UTC, b) 04.10.2016 12:00 UTC and c) 05.10.2016 12:00 UTC

5.2 Observations

5.2.1 Model vs observations

In this section I will present comparison between model results and observations obtained with the dropsondes released during the NAWDEX field campaign. This comparison acts as a more qualitative model validation, complimentary to section 5.1. I have chosen the dropsondes on the basis of their respective research aim i.e the ones released into WCB outflows or into ARs (EPATAN (2016)), since these are the most relevant weather systems to this thesis and comparison will therefore yield the most beneficial result. The dropsondes released from flights RF10, RF11, RF13 and RF14 will be presented as crossections of mixing ratio [g/kg] calculated from vertical profiles. Data from flight RF12 will be presented as the raw vertical profiles based on the flighttrack and dropsonde location. The dropsondes have some incidents of obeservational errors where values of mixing ratio is either measured extremely high or low compared to it's surroundings measured values. This is identified as vertical lines of off-colored shadings in the figures of vertical crossections of mixing ratio. See Figure 3.1 for all dropsonde locations and Table 3.1 for flight number and dropsonde release time.

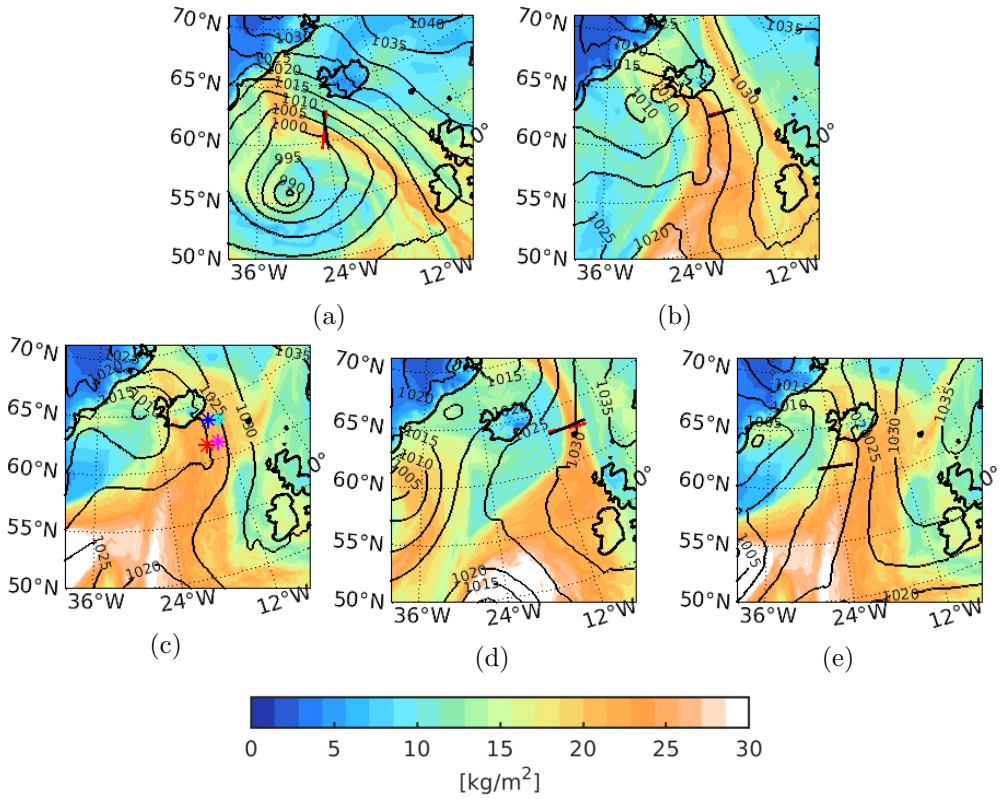

Figure 5.4: TCWV(shading; kgm^{-2}) and MSLP(contours; hPa) from run010 at a) 07.10.2016 15:00 UTC, b) 09.10.2016 12:00 UTC, c) 09.10.2016 18:00 UTC, d) 10.10.2016 12:00 UTC and e) 11.10.2016 18:00 UTC. The black and red line in a),b),d) and e) highlightes the region for the crossection made from model results and from observations, respectivly. The colored (*) markers in c) indicate dropsonde locations

Flight RF 10, 07.10.2016

During flight RF10 (5.4 a), seven dropsondes were released into and across the airflow of a relatively weak AR located southwest of Iceland (EPATAN (2016) Flight Reports). A clear separation is apparent between the moist regions inside the AR (D2 - D6) from 600 - 800hPa, and the drier regions outside the AR (D1 and D7) in figure 5.5 a). This separation is not resolved by the coarse resolution model run050 (Figure 5.5 b). Here the water vapor is more evenly spread, and does not have the characteristic plumelike feature of the AR. Model run010 resolves the AR's vertical structure to a greater degree. In figure 5.5 c) a clear separation is evident between the moist regions inside the AR and the drier regions outside the AR in approximate corresponding locations to Figure 5.5 a. Quantified values of specific humidity in both model runs are in over all agreement compared with observations and show similar vertical water vapor distribution. Values of range from 7 g/kg near 1000hPa and 2 g/kg near 600hPa, where the latter seems to be the roof or the top of the AR.

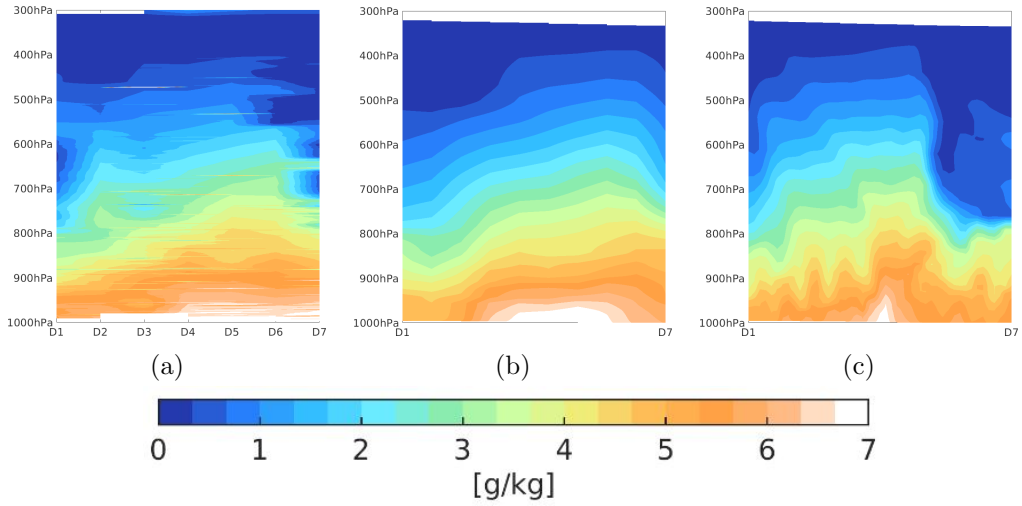

Figure 5.5: a) Crossection of mixing ratio(shading;g/kg) from dropsondes from flight RF10. The values have been interpolated between the vertical profiles gathered by the dropsondes. b) Crossection of specific humidity in corresponding dropsonde locations from coarse resolution model run050 at +159h leadtime. crossection of specific humidity in corresponding dropsonde locations from fine resolution model run010 at +159h leadtime.

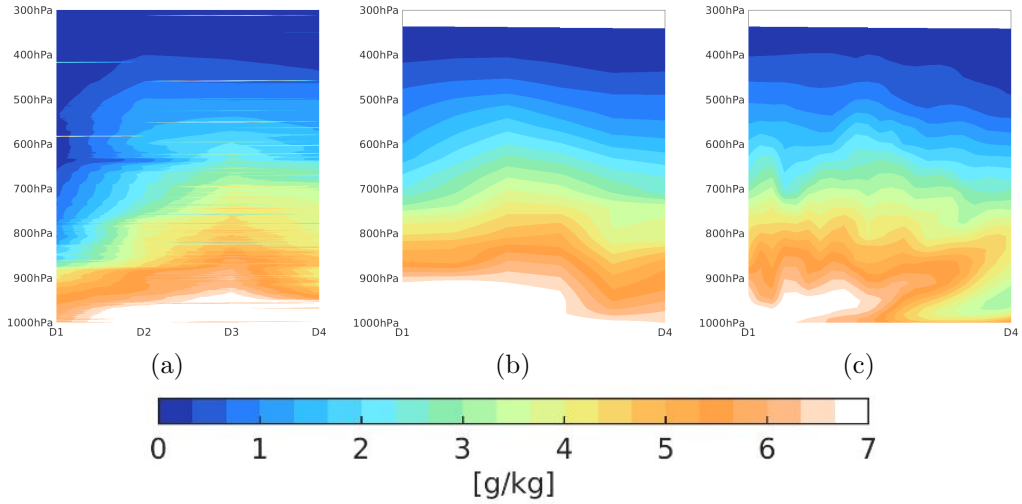

Figure 5.6: Same as figure 5.5 but a) is for flight RF11 and b-c) is for +204h leadtime

Flight RF 11, 09.10.2016

During flight RF11 (5.4 b), four dropsondes were released into and across the airflow of the WCB associated with the third cyclone. Over all the vertical distribution is well resolved from both the model runs with the exception near the western edges of the crossection (D1). However, one difference is indicated in Figure 5.6 c) near D4, where moist air with values of around 5-6 g/kg is being situated above (850 hPa) drier air with values of around 3 g/kg (900-1000hPa). Indications of this can also

be seen from the dropsonde observations (Figure 5.6 a), but to a lesser extent and is not resolved by run 050.

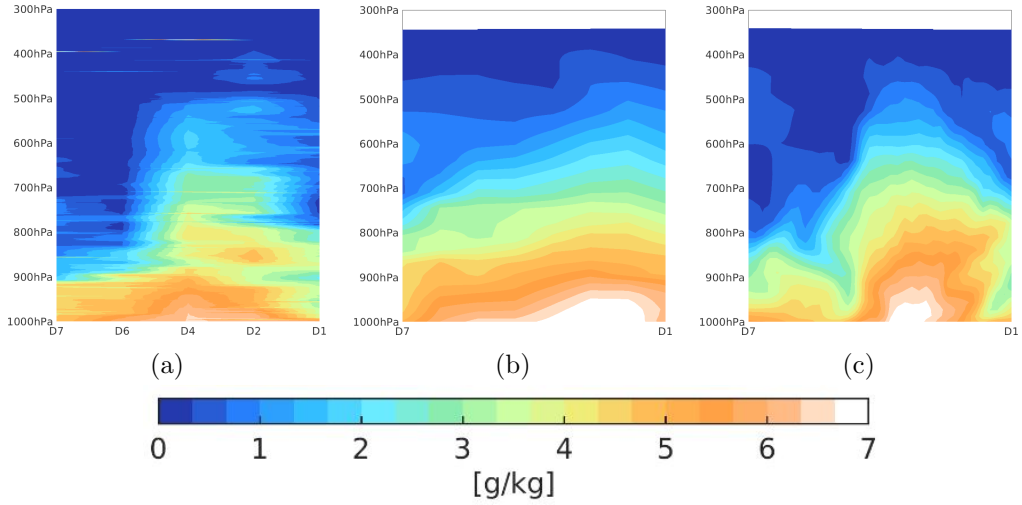

Figure 5.7: Same as figure 5.5 but a) is for flight RF13 and b-c) is for +228h leadtime

Flight RF13, 10.10.2016

During flight RF13, seven dropsondes were released into an AR associated with cyclone 3. An overview of TCWV distribution and area for the crossection is shown in Figure 5.4 d). Two of these dropsondes had instrumentation errors and are not taken into account for the calculation of the crossection. Results from run050 do not have well agreement with observations and no clear vertical structure can be interpreted from this (Figure 5.7 b). The dropsonde results (Figure 5.7 a)) shows the distinct vertical structure of moisture in the AR, stretching up to 500 hPa from D4-D2. The sharp edge of the AR near D6, descends to 900hPa. This vertical distribution of moisture is well represented by model run010 (Figure 5.4 c). The top of the AR is situated at around 500hPa in both run010 and the observations. The specific humidity near the surface in run010 is more concentrated in the center of the AR with values of over 7 g/kg, compared to the dropsonde results with values of around 6 g/kg. One possible explanation for this is that the dropsondes might not have been exactly inside the center of the AR, since this region is very narrow.

Flight RF14, 11.10.2016

During flight RF14, four dropsondes were released into the outflow of the WCB, located south west of Iceland. The horizontal TCWV distribution from run010 (Figure 5.4 e), shows that the water vapor is evenly spread out. From the same figure it is evident that the crossection is at the western edge of the this moist region. The crossection made from dropsonde observation (Figure 5.8 a) has an even vertical distribution of moisture with small horizontal differences. The crossecstion from model run010 (Figure 5.8 b) does not reproduce this even distribution with values ranging from 4.5g/kg near the western edge of the crossection and to 7g/kg

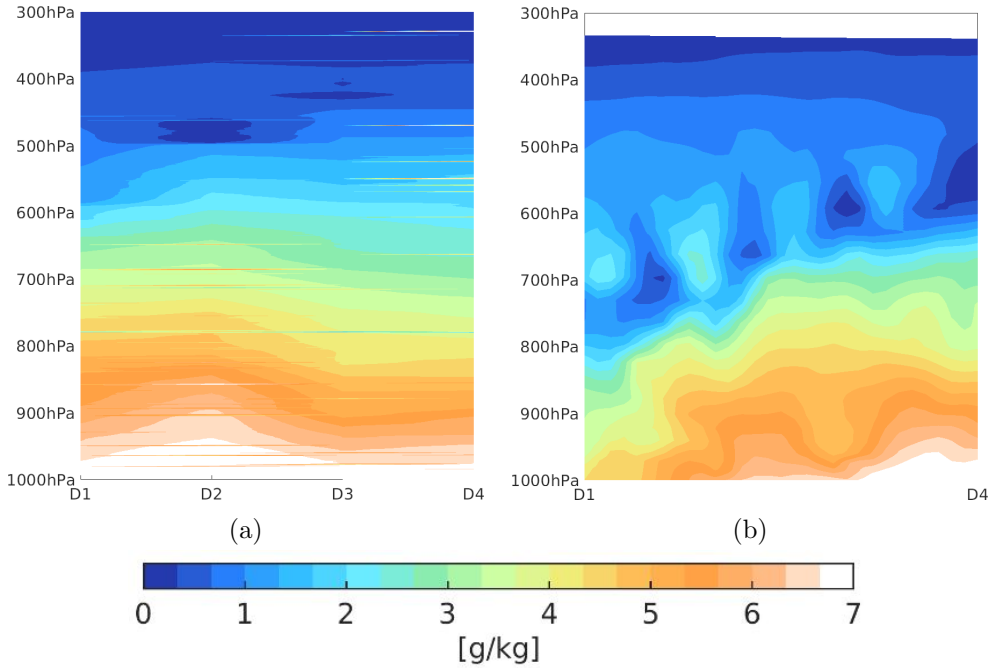

Figure 5.8: Same as figure 5.5 but a) is for flight RF14 and only model results from run 010 and b-c) is for +258h leadtime

at the eastern edge, at 1000hPa. The most notable feature from the model run010 is the wave-like pattern at 650 hPa. This pattern is not apparent in the observed values of mixing ratio 5.8 a.

Flight RF12, 09.10.2016

During flight RF12, two pairs of dropsondes were released during two crossections of the WCB outflow south of Iceland(Figure 5.9 a). The largest distinction between the profiles of mixing ratio are that dropsondes D1 and D4 observed substantially drier regions of the atmosphere under 600 hPa compared to D2 and D3. D4 reaches moister regions again at around 800 hPa, while D1 gives much lower values of $2g/kg$ from 600 - 870 hPa. Based on the satellite image in the EPATAN flight report it seems that both D1 and D4 were released into seemingly moist regions. Observed values of mixing ratio indicate that these two dropsondes were occupying regions outside the WCB. Slight indications of this is identified by the coarse resolution, run050 profiles (5.9 b). However, only from around 750 hPa to 850 hPa. Notably, the higher resolution run010 (Figure 5.9 c) does not resolve this region of drier air. All vertical profiles from both model runs are in overall agreement with the D2 and D3 dropsondes, with the exception being the D4 vertical profile from run010 below 900 hPa. Here the model is simulating a region of drier air (4 g/kg) compared to D1,D2 and D4 (6-7.5 g/kg).

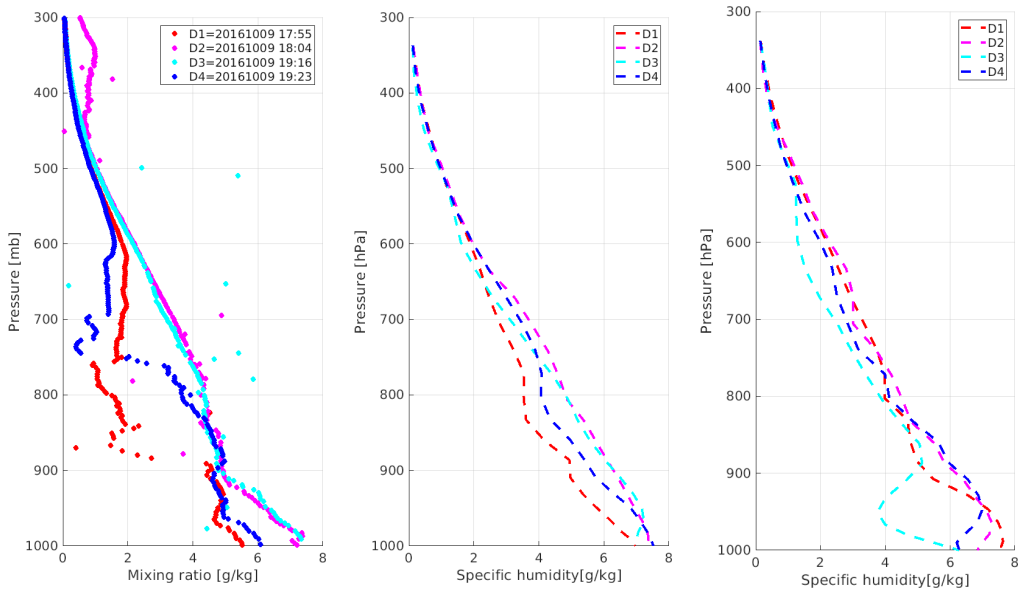

(a) (b) (c)

Figure 5.9: a) Vertical profiles of mixing ratio obtained from dropsondes released during flight RF12. b),c) vertical profiles of specific humidity in coresponding dropsonde locations from COSMO runs 050 and 010 respectively.

Comparison between observations obtained from dropsondes and model results from the runs, run050 and run010 reveals an overall agreement in distribution of water vapor. Notably, at higher resolution (run010) the model resolves the vertical structures of the ARs excellently. Run050 resolves the vertical structure of the AR investigated by flight RF10, but there is little agreement between the run050 and the observations obtained from flight RF13. Comparison between the model and the observations made from flight RF11 investigating the WCB outflow (Figure 5.6) are in agreement concerning vertical distribution of moisture. Run010 resolves the dry air intrusion occurring near the eastern edge of the crossection that is evident in the observations. Results from run010 on the 11.10.2016 however, has a wave-like pattern at 700hPa that is not indicated from dropsonde results, and shows poor agreement overall.

5.3 Moisture origin in water vapor and precipitation

To identify the moisture origin of water vapor associated with the extratropical cyclones present during the period of the NAWDEX field campaign, I have separated the water vapor associated with cyclone center proximity and the frontal system of the respective cyclone and applying the water vapor tagging feature (section 3.5). The separation of water vapor from the different weather systems is done by summation of each individual water vapor tracer in the "Cy1/Cy2" domain and the "AR1/AR2" domain, respectively (Figure 3.2). All tracer contributions have been compared to the total amount of TCWV and presented as a timeseries of the fraction of the total amount of water vapor, called "water vapor" or "precipitation budgets".
Water vapor contributions from all the different water vapor tracers have been calculated in the same domain as the handover of moisture for intercomparison (Chapter 5.5).

Here I give a description of the water vapor tracers that make up the water vapor budget associated with the three cyclones; A, B and C. This analysis is based on COSMO model results from run010, which in section 5.2 showed to reliably represent AR structures.

Budgets for cyclone center proximity

Figure 5.10 shows the timeseries of water vapor source fractions for cyclone center proximity. The black crossed line (hPa) indicate the temporal evolution of the cyclones lifespan, where the troughs show the minimum pressure of the respective cyclones. The SEvap tracer has uniform distribution (50%) through the lifespan of all the cyclones but then decreases to near 30 % towards the end of the simulation, simultaneously as the western tracer, W (yellow) increases to 60-70%. During the lifespan of Cyclone A (01.10 12:00 - 04.10 00:00), the sources from the lateral boundaries (N/E, W and S) have not had enough time to be advected into the Cy1/Cy2 domain. Therefor the largest source contributions are from the IA tracer as well as the SEvap tracer. Upwards of 80% of total water vapor is explained by this tracer during the early stages of the cyclone (02.10 00:00), while 40% during the later stages (03.10 12:00). Since IA is the largest contributor the water vapor associated with Cyclone A, it is not traceable to any of the water vapor sources.

During the lifespan of the second cyclone (04-06.10.2016) only 5-7 % of the IA tracer is left in the domain. Now the Western tracer, W (yellow), is contributing substantially with values above of 30-40 % throughout the whole lifespan Cyclone B. 1-2 % of the eastern tracer, N/E (orange) is identified as well in Cyclone B. The southern tracer, S (purple) contribute only to less than a percent during Cyclone B's lifespan.

For the third and substantially weaker cyclone (07-09.10.2016), large amounts of the western tracer,W is substituted by the eastern tracer N/E. Fraction of W decreases

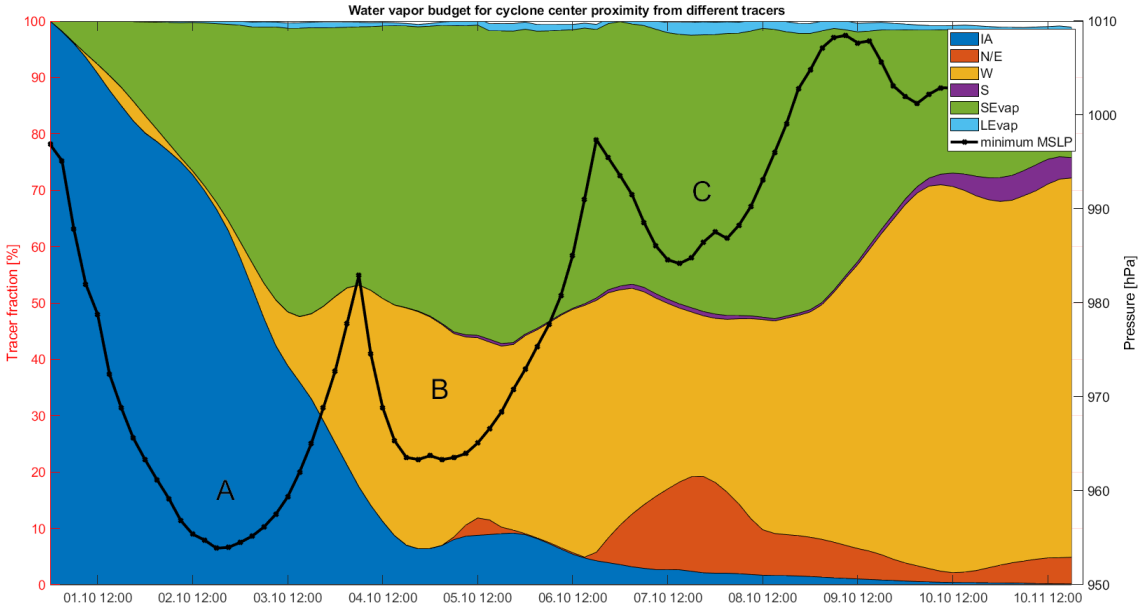

Figure 5.10: Time series of water vapor source contribution for cyclone center proximity (Boxes Cy1/Cy2 in figure 3.2). Colored areas show tracer contribution [%] to the total amount of water vapor in the respective box. The tracers IA (blue), N/E(orange), W(yellow), S(purple), LEvap (light blue) and SEvap(green) are shown. The black and crossed line is showing minimum MSLP(hPa) in the Cy1/Cy2 box. Capital letters A, B and C denote respective cyclone periods

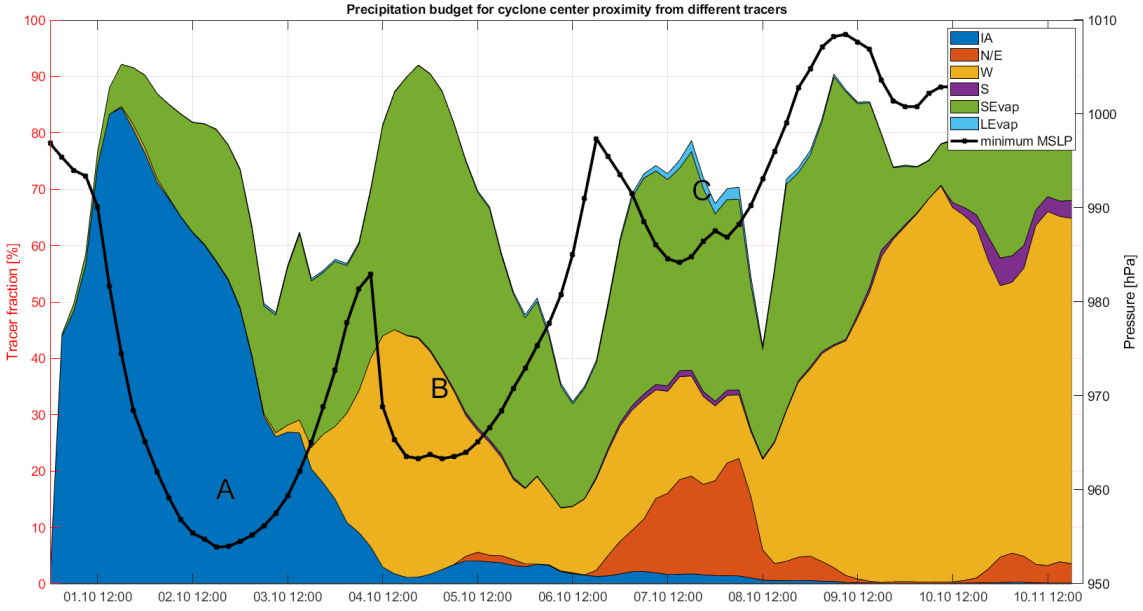

Figure 5.11: Same as Figure 5.10 but for precipitation tracer contribution.

to 25-30% while N/E increases from 0-15 %. This can be partly explained by the orientation of the AR located to the east of the Cy1/Cy2 box (see Figure 4.1 g))

that is transporting water vapor into the vicinity of Cyclone C's center

The tracer contributions to the precipitation associated with the cyclones (Figure 5.11) exhibit a much stronger temporal variation than the water vapor budget and a strong increase in precipitation amount during each cyclones duration. However the distribution of fractions for precipitation contribution show a similar pattern as to the water vapor budget. During the lifespan of the second cyclone the largest contributions are from SEvap (45 %) and W (35-45 %). For the third cyclone the N/E tracer actually exceeds the contributions from W, but only by about 5 %. This is none the less a notable incident since the western tracer, W, contributes with values of around 35% while the eastern tracer, N/E has values of around 15% in the water vapor budget (figure 5.10). One explanation for the precipitation budgets not being closed (not 100%) is that the tagged water vapor is only from the variable,large scale accumulated precipitation, and it is being compared with the total precipitation which includes , large scale accumulated precipitation, convective precipitation and snow fall.

Budgets for front and AR proximity

The water vapor budget for the "AR1/AR2" domain (see figure 3.2), associated with water vapor from the frontal structure of the cyclones and the ARs (Figure 5.12) show the tracer fraction contributions to the total amount of TCWV in the domain. The black and crossed line show the minimum MSLP in the "Cy1/Cy2" box, since it is in this box the cyclone center is located. Two similarities between the two budgets are the even distribution of the SEvap tracer throughout the simulation and the lifespan of the IA tracer. The IA tracer reaches values of around 10% at 04.10.2016 in both domains. The contributions from the different tracers for the "AR1/AR2" domain are remarkably different from the "Cy1/Cy2" domain. This can partly be explained by the greater meridional extent of "AR1/AR2" domain since parts of the southern tracer, S, is advected directly into the domain and the N/E needn't travel as far westward to reach the domain. Two similarities between the two budgets are the even distribution of the SEvap tracer throughout the simulation and the lifespan of the IA tracer. The IA tracer reaches values of around 10% at 04.10.2016 in both domains.

Contrary to the sources in the vicinity of cyclone A's center, in the "AR1/AR2" box parts of the water vapor is traceable to known sources. Even during the early stages of the cyclone, above 10% of water vapor is contributed by the southern tracer, S. At the later stages, both S and N/E tracers are contributing near equally with 10-12%. The distribution of the tracers S an N/E are similar during Cyclone B's lifespan with contributions of 10-15% and the western tracer, W being the dominant lateral source contributions with 20-25%.

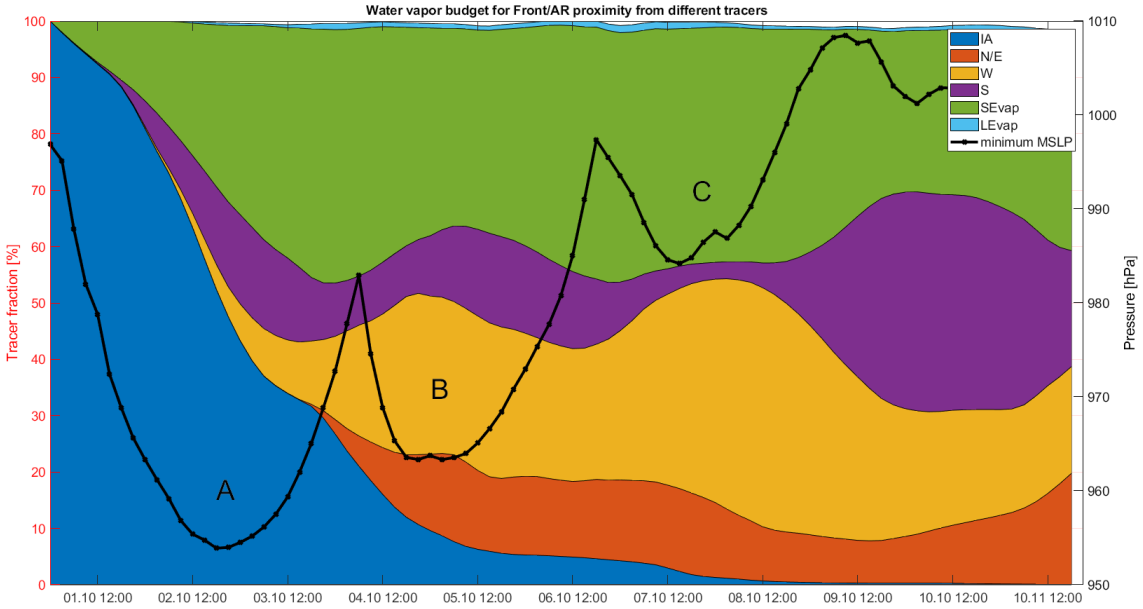

Figure 5.12: Same as for Figure 5.10 but for the front/AR proximity domain AR1/AR2 (Figure 3.2)

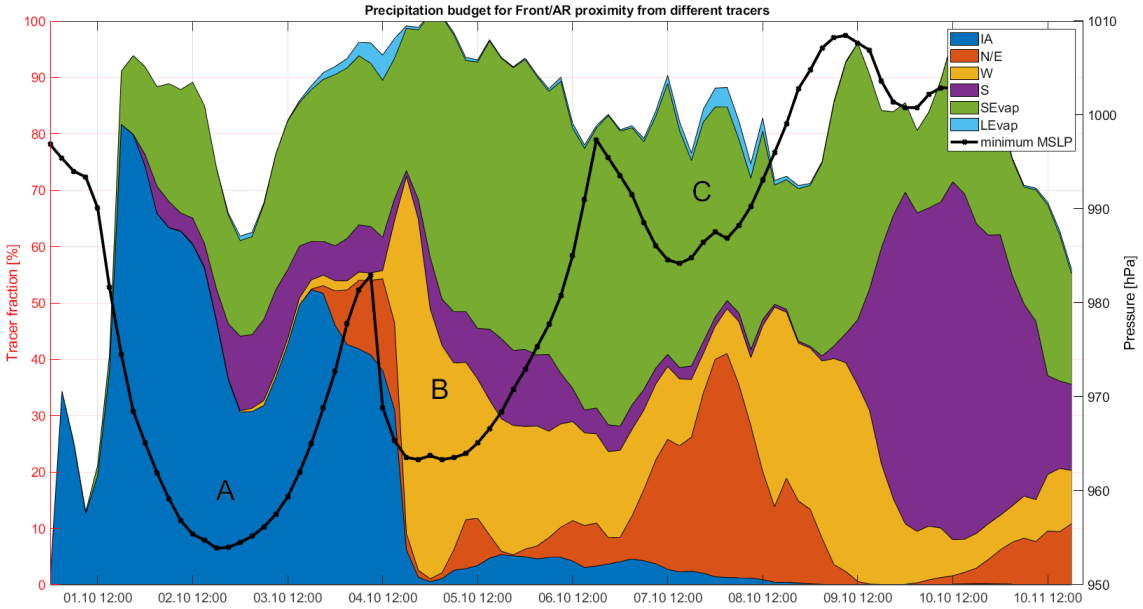

Figure 5.13: Same as for Figure 5.10 but for precipitation tracer contribution in the front/AR proximity domain AR1/AR2 (Figure 3.2)

One clear distinction in the distribution of water vapor sources in extratropical cyclone have been identified from this analysis. Water vapor associated with cyclone center proximity is predominantly from sea surface evaporation and the tracer W. The southern tracers have virtually no contributions throughout the research period while the N/E tracer as a small peak during Cyclone C's lifespan (Table 5.1). The water vapor associated with the frontal system of the respective cyclones show a much more even distribution of all the lateral water vapor sources. However sea surface evaporation is dominating all the other sources (Table 5.2). The precipitation budgets show a substantial increase in precipitation amount during cyclone periods but the distribution of precipitation contributions from the different tracers follow the distribution of water vapor sources closely.

Table 5.1: Average fraction contributions [%] in the Cy1/Cy2 box from water vapor sources during the lifespan of Cyclone B and Cyclone C

	IA	N/E	W	S	SEvap	LEvap
B	8.3	0.6	38.2	0.2	51.4	0.8
C	2.3	10.3	36.2	0.6	48.7	1.6

Table 5.2: Average fraction contributions [%] in the AR1/AR2 box from water vapor sources during the lifespan of Cyclone B and Cyclone C

	IA	N/E	W	S	SEvap	LEvap
B	8.7	12.5	25.4	12.7	39.5	0.8
C	2.0	12.2	35.6	6.7	42.0	0.9

5.4 Vertical distribution of water vapor tracers

In this section the vertical distribution of water vapor tracers based on the high resolution model run010 are presented. Results are presented as vertical distribution of water vapor tracers in corresponding crossections to the ones obtained from the observations from the dropsondes released during flight RF10,RF11,FR13 and RF14. The vertical distribution of water vapor tracers in these locations have been chosen since comparison between model run01 and observations showed that the model resolved the observed AR events excellently, and the WCBs over all well (section 5.2). Thus it is reasonable to assume that the distribution of water vapor tracers from model results represents the actual distribution of water vapor source contribution in the real atmosphere. Tracer contributions are presented as a fraction [%] to the specific humidity (g/kg). The results presented here show the tracers N/E, W and S. The SEvap tracer has been excluded because of it's dominant contribution throughout the crossections. Additional figures including the SEvap tracer can be found in the Appendix A.4

AR south of Iceland 07.10.2016

During the 07.10.2016 an AR located south of Iceland were investigated by the SAFIRE Falcon aircraft. Comparison between model results and observations showed excellent agreement of vertical distribution of moisture between model run010 and the observations obtained from the dropsondes (section 5.2).
Horizontal distribution of tagged TCWV show that of the lateral tracers are present in the crossection (Figure 5.14 a, b, c). The N/E and W tracer are distinctly separated in the north and the south of the crossection. However, note the difference in colorbar scale in Figure 5.14 a,b and c. This is also evident in the vertical tracer distribution in figure 5.14 e) where the tracers are separated in the middle section of the AR at the contour line of 10% . At higher and drier altitudes above 600 hPa, the W tracer has a stronger contribution even at the northern side. The southern tracer S is only found residing at high altitudes above 450 hPa and only with a 10% contribution. This is a very dry region with specific humidity values of around 0-1 g/kg so the concentration of this tracer is contributing very little to the total TCWV.

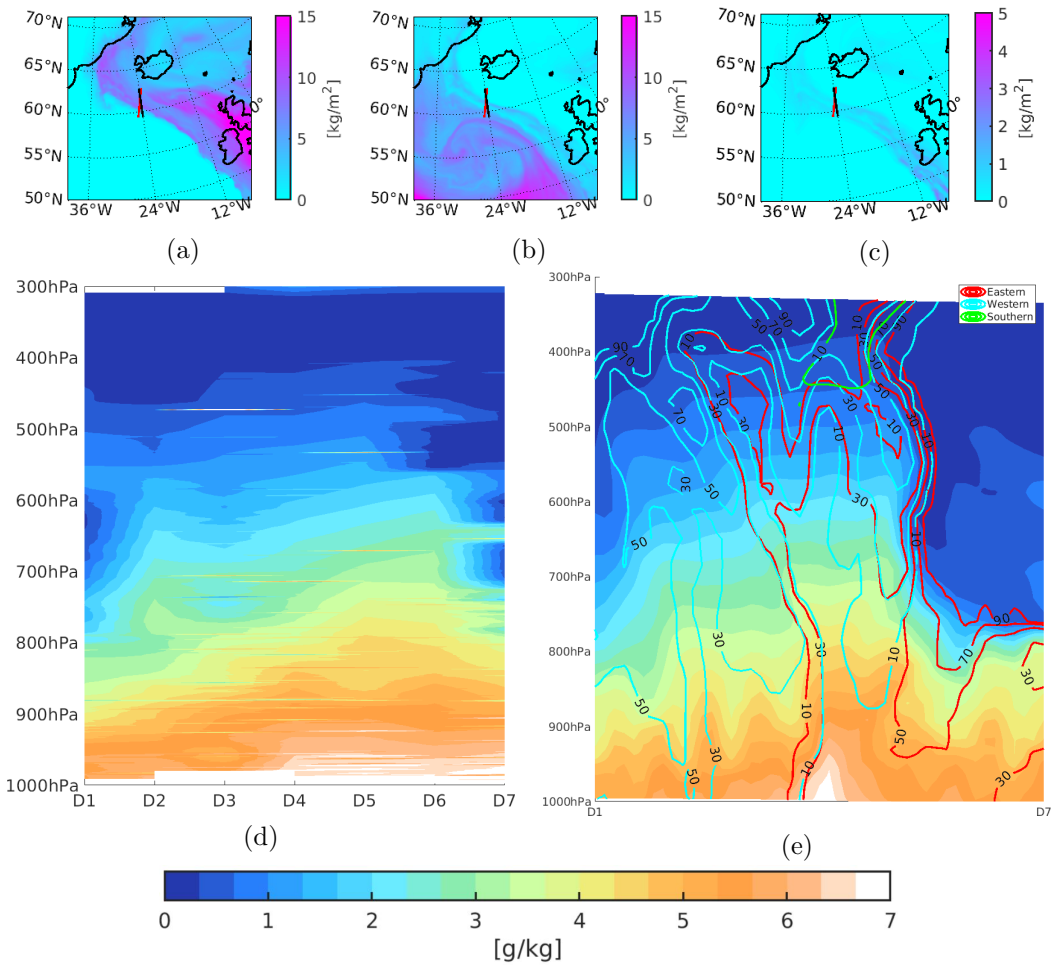

Figure 5.14: TCWV contributions from the tracers a) N/E, b) W and c) S at 07.10.2016 15:00 UTC from run010. Black line highlights area for the crossection made with model results, red line highlights crossection based on dropsonde data. d)Veritcal crossection of mixing ratio (shading;g/kg) interpolated from vertical profiles gathered from dropsondes. x-axis shows corresponding dropsonde. e) Crossection of specific humidity(shading;g/kg) from COSMO run010. The crossection has start and end points at first and last dropsonde locations, respectively. Contours show tracers fraction [%] from lateral boundaries sources (N/E;red,W;Cyan and S;Green). Tracer fraction is compared with total amount of specific humidity in the crossection.

WCB outflow south of Iceland, 09.10.2016

Flight RF11 investigated a WCB located south of Iceland on 09.10.2016. From section 5.2 we saw that the vertical distribution from crossections of mixing ratio from dropsonde observations were in fairly well agreement compared with specific humidity from the model run010. The horizontal distribution of tagged TCWV indicate that only the western tracer,W is contribution above 10% to the crossection (Figure 5.15 a), b) and c). W has a strong contribution of 50% of total water vapor in the middle section of the WCB from the surface up to 650hPa.

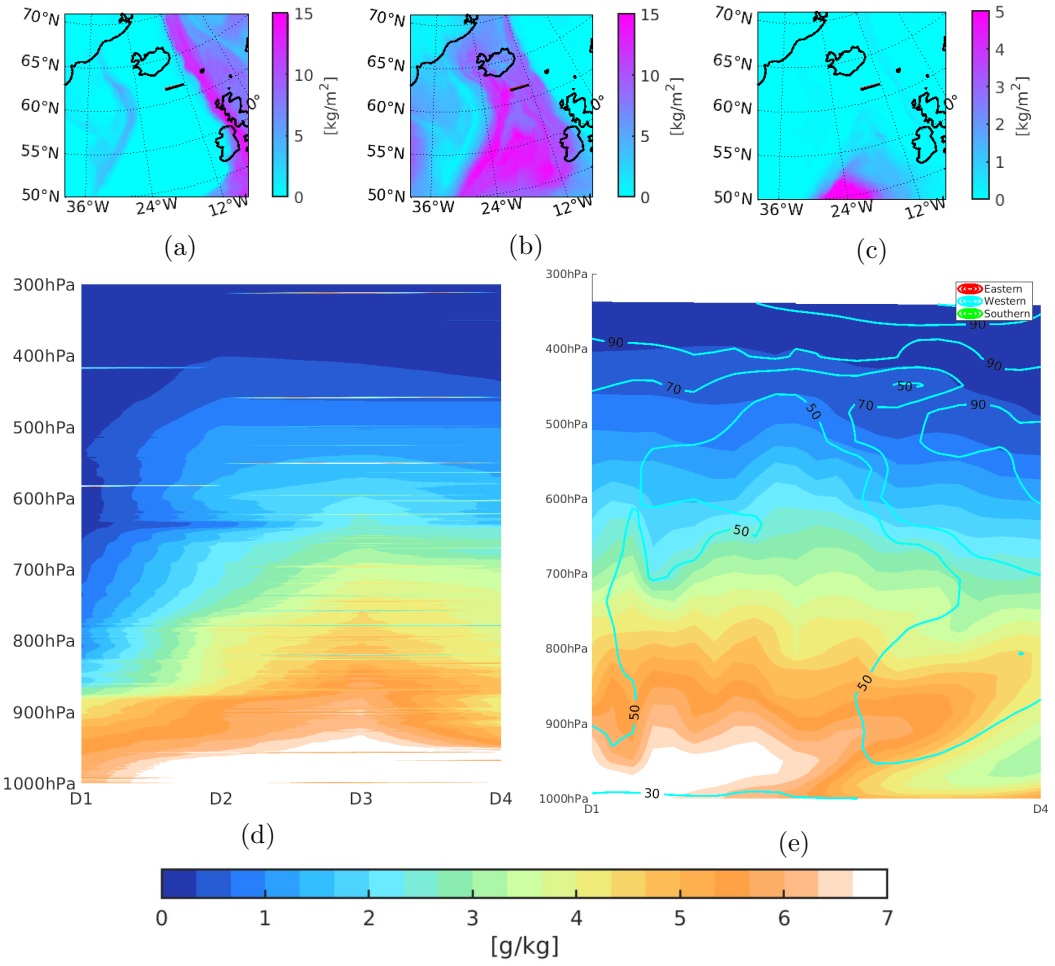

Figure 5.15: Same as figure 5.14 but d) is for flight RF11

AR east of Iceland 10.10.2016

Flight RF13 investigated the AR associated with the third cyclone, located east of Iceland on the 10.10.2016. Comparison of crossections between observations of mixing ratio from dropsondes and specific humidity from model run010 show an excellent agreement in vertical distribution of moisture (Figure 5.2). The horizontal distribution of tagged TCWV from the the lateral boundaries (Figure 5.16 a), b)

and c)) show that all three tracers are present in the crossection. One notable feature from the tagged TCWV from the N/E source is that it is present in both ends of the crossection. From figure 5.16 a) we see that the TCWV in the region near the crossection has a spiraling shape north of Iceland and it loops around the east of Iceland again and where parts of this is ends up in the western part of the crossection. The water vapor associated with this is predominantly at lower levels from 800 - 1000 hPa, with values of 10% an located west of the AR. The AR itself has the strongest contribution from the western tracer, W, throughout it's vertical extent. However, eastern parts in the lower levels of the AR (900 - 1000 hPa) have a substantial contribution from the N/E tracer, as well as near the core of the AR where N and N/E are equally in contributions (around 30%). The southern tracer,S is only residing at higher altitudes of the AR, but with low contributions of 10% in regions with specific humidity values ranging from 0-2 g/kg.

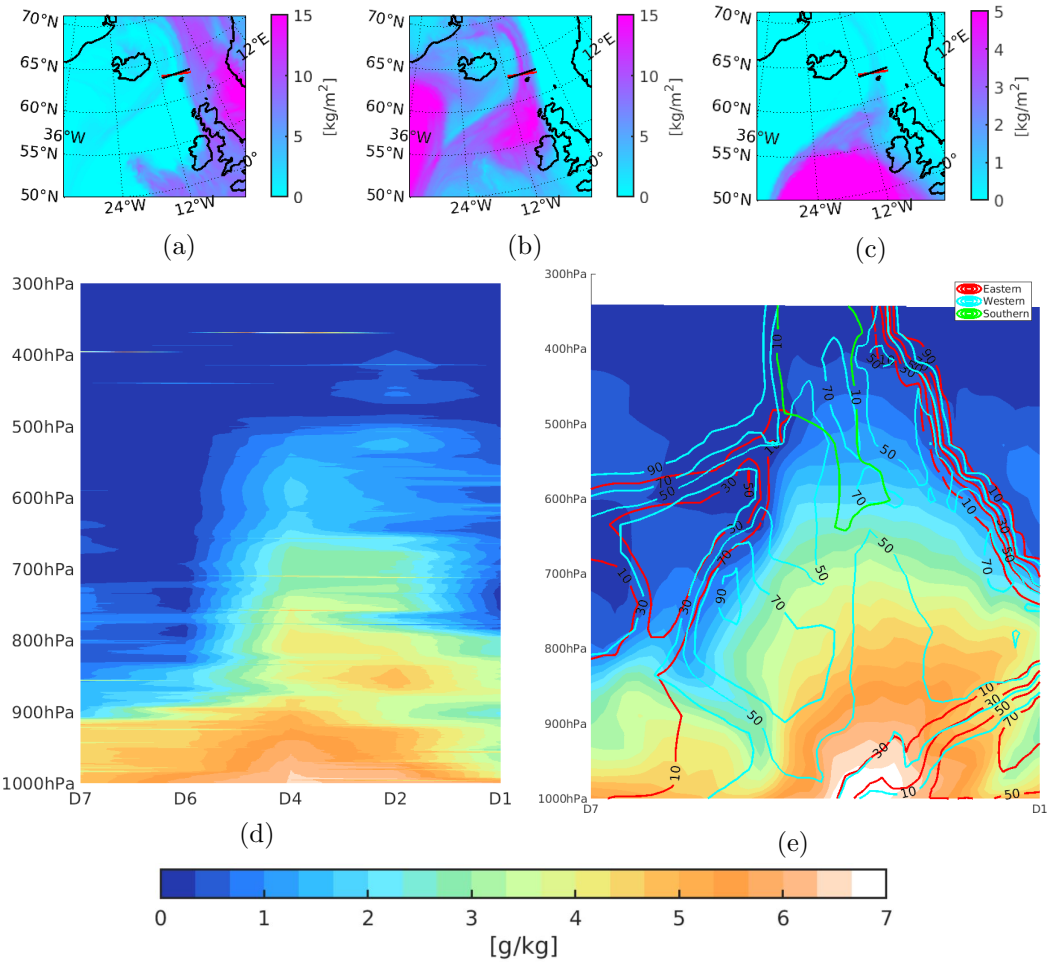

Figure 5.16: Same as figure 5.14 but figure d) is for flight RF13

WCB south west of Iceland 11.10.2016

Flight RF14 investigating the outflow of the WCB located south west of Iceland on the 11.10.2016. Comparison between crossection of mixing ratio from observations and specific humidity from run010 show poor agreement especially because of the the wave pattern at 650 hPa in the model results. From figure 5.17 a-c) we see that the horizontal tagged TCWV is from all sources are present in the crossection. The eastern tracer is only located at lower levels at the eastern most part of the crossection with contribution of 10% close to the surface. The southern tracer, S, is also contributing to the eastern part of the WCB also with values around 10%. Notably with a much larger vertical extent and in a moist region from the surface up to 800 hPa where specific humidity values range from 5-7 g/kg. The rest of the crossection is dominated by the western tracer, W, with values reaching as high as 90% even at lower and moist levels (950 hPa).

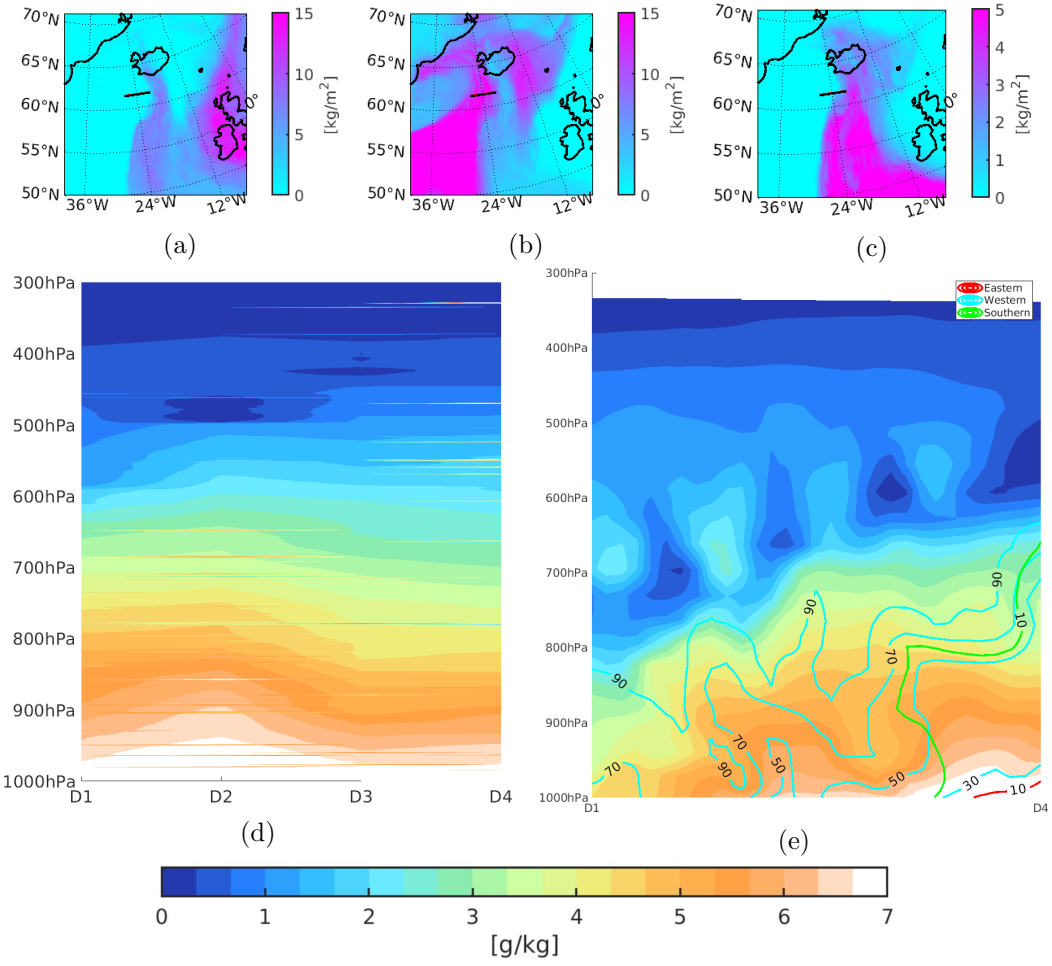

Figure 5.17: Same as figure 5.14 but figure d) is for flight RF14

5.5 Quantifying handover of moisture

In this section I address the quantification of moisture handover between extratropical cyclones. During the 11-day research period a total of 3 extratropical cyclones are identified in the domain. This allows the phenomenon of handover of moisture to potentially occur two times. To investigate this, moisture tracers are released in a 3-hour period at two different time steps, during Cyclone A and Cyclone B minimum pressure. This tagging of cyclone moisture acts as a "snapshot" of the cyclones total moisture. Thereby, we distinguish the water vapor associated with the cyclone's center and its frontal structure. The weather situation for the two different time stamps can be seen in figure 5.18 a) and b). The red box shows the area where the tracers Cy1 and Cy2 are released, while the blue boxs shows there the tracers AR1 and AR2 are released. In the blue box in figure 5.18 b) we see both the moisture associated with the second cyclones frontal structure from 55 - 40 ^oN as well as the remnants of the AR associated with Cyclone A at 60 ^oN, meaning that parts of the water vapor associated with the first tracer initialization(AR1) is tagged an additional time and given a new tag (AR2).

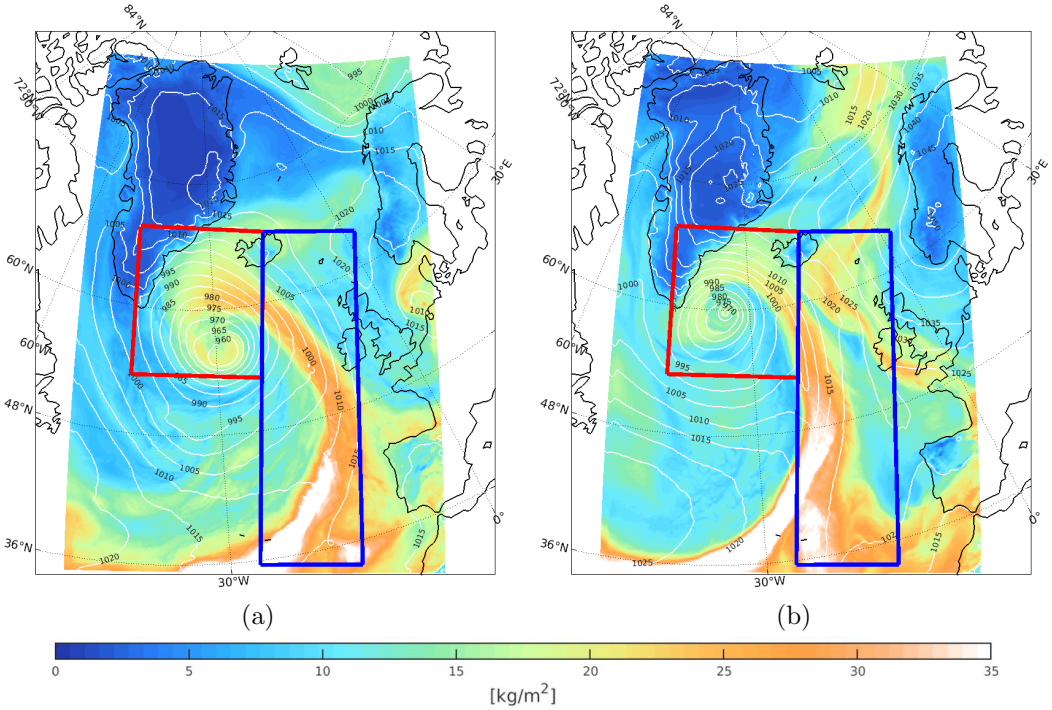

Figure 5.18: TCWV and MSLP for a) tracers Cy1 and AR1 release time; 02.10.2016 15:00 UTC and b) tracers Cy2 and AR2 release time; 05.10.2016 09:00 UTC. Red and blue line highlights the area covered by the Cy1/Cy2 and AR1/AR2 boxes, respectively (See figure 3.2).

The results here are presented as water vapor and precipitation budget timeseries from the water vapor tracers released from the two boxes. This is done to highlight if the water vapor that is being handed over to a successive cyclone is being used (i.e. being handed over) to generate precipitation.

Water vapor and precipitation in the "Cy1/Cy2" domain

Figure 5.19 shows the time series of the fractions of the handover tracers Cy1,Cy2,AR1 and AR2 compared to the total TCWV in the Cy1/Cy2 domain. Each tracer present in domain is averaged and represented as one value per 3 hour. This means that the tracers located outside the box after tracers-initialization is not taken into account in the water vapor or precipitation budget. Shortly after initialization of the tracers Cy1/AR1 (2.10.2016 15:00 UTC) and Cy2/AR2 (5.10.2016 09:00 UTC) and the water vapor budgets exceeds contributions of 100%. This is because the AR tracers are being transported into the Cy1/Cy2 domain shortly after initialization as well as the tracer contributions are stacked on top of each other. The black dashed lines highlights the period for which the tracers are released. As previously mentioned, the tracers are only released in a 3-hour period and leads to the rapid removal of tracers due to precipitation and advection out of the domain. The first incident of handover of moisture can be identified from the period 04-06.10.2016 where contributions of 10% of the tracer Cy1, associated with Cyclone A, is identified in the domain during Cyclone B's lifespan. The Cy1 tracer even has a secondary peak in concentration during the later stages of the cyclone. By analysing horizontal tracer distribution during this period it is seen that this is largely due to the Cy1 tracer being advected westward out of the Cy1/Cy2 domain in the later stages of Cyclone A, and then being reincorporated into Cyclone B's air flow. Smaller amounts of AR1 can also be identified in Cyclone B, however only a few percent (1-3%) are present. Because little water vapor from AR1 is transported into the Cy1/Cy2 domain, parts of this moisture is left behind in the AR1/AR2 domain and remains potentially available for interaction with Cyclone C.

Cyclone C have contributions from both the Cy2 and the AR2 tracer. Contrary to the Cyclone B, here the AR2 tracer is the largest contributor in the handover process with 10-15% where as the Cy2 has contributions around 3-5%. The is can partly be explained by the AR orientation during Cyclone C's lifespan. The AR is oriented into the cyclones center and therefore favors north westward transport of water vapor(Section 4.1 ,figure 4.2 a)

Precipitation from the tracers Cy1, AR1, Cy2 and AR2 (Figure 5.20) occurs predominantly during the lifespan of its associated cyclone. However,tracer contributions to precipitation are also evident in both incidences of the handover process. Contributions to precipitation from Cy1 is identified during the later stages of Cyclone B, but only small amounts of 1-2% in the period 05-06.10.2016. Very small amounts of AR1 tracers are also identified here (1-2%). The by far greatest contribution to precipitation are from the AR2 tracer during Cyclone C. AR2 contributes 15-20% of total precipitation during major parts of Cyclone C's lifespan (06.10.2016 15:00 UTC - 08.10.2016 09:00 UTC). The tracer Cy2 also has a contribution of around 5-7% during the early stages of Cyclone C.

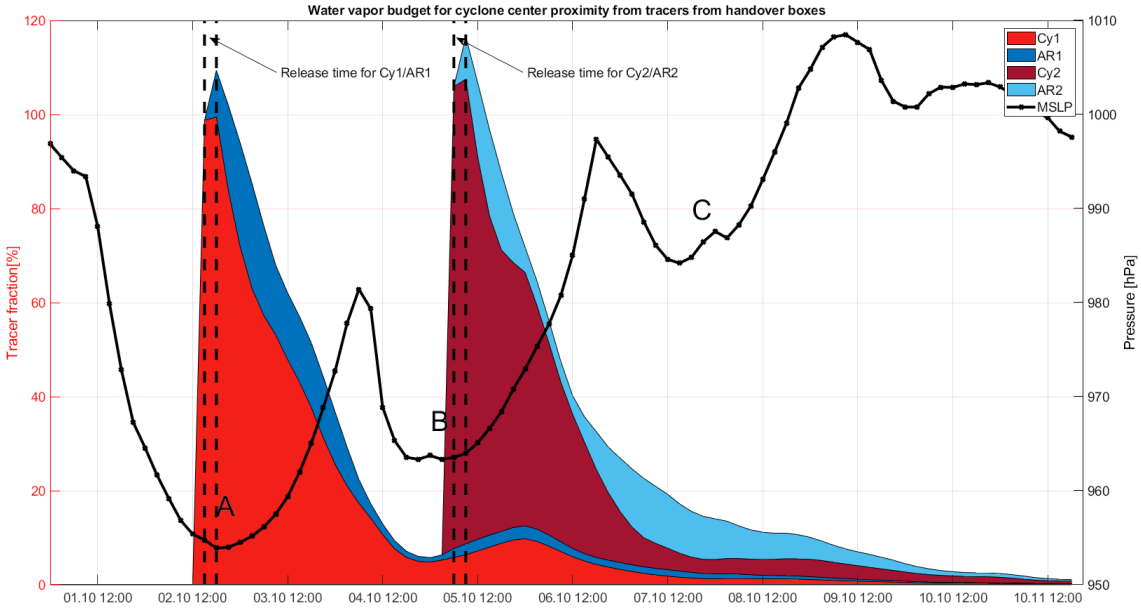

Figure 5.19: Water vapor budget for cyclone center proximity(Cy1/Cy2 handover box, figure 3.2) for water vapor tracers for the time period 01-11.10 2020. Colored areas show water vapor tracers, quantified as a fraction (%) compared to total TCWV in the respective box. Tracers from Cy1 (Red),AR1 (Blue), Cy2 (Dark red) and AR2(Light blue) are shown. The black solid and crossed line show the minimum MSLP in the Cy1/Cy2 box (Right y-axis[hPa]). Capital letters A, B and C denote cyclone periods

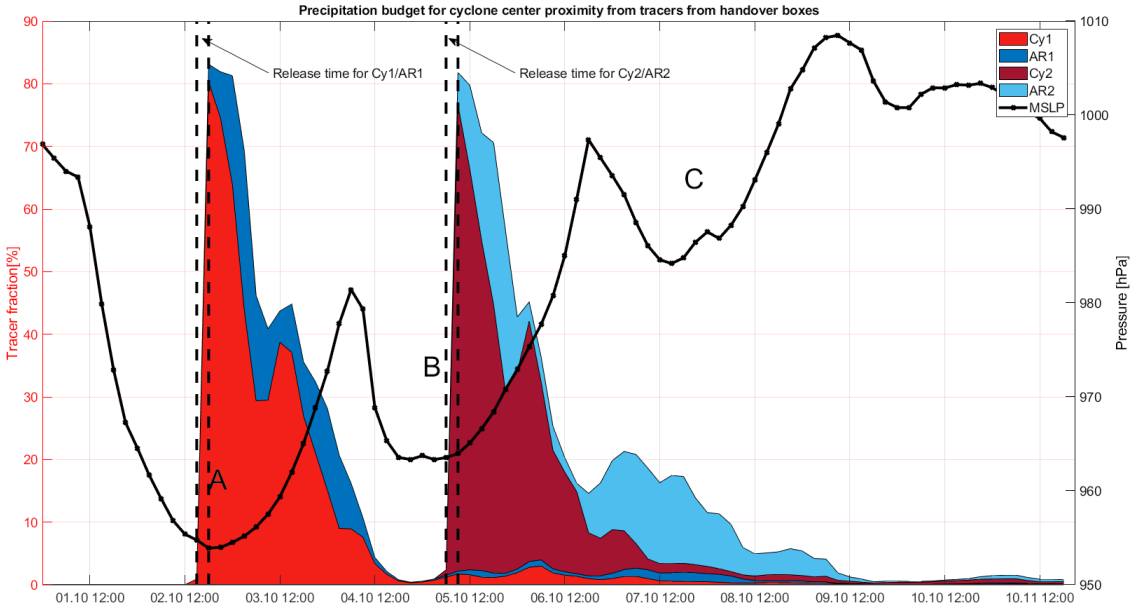

Figure 5.20: Same as Figure 5.19 but for precipitation

Water vapor and precipitation in the "AR1/AR2" domain

Now, the water vapor tracers associated with the cyclone's frontal structure are analyzed to investigate the importance of water vapor transport in the ARs to the handover process. Figure 5.12 show the tracer fractions in the AR1/AR2 domain (blue box in figure 5.18) as a timeseries in the period 01-11.10.2016. Right after the initialization the tracers are rapidly removed from the domain, by either advection or precipitation. This is similar to the tracers for the cyclone center proximity budget. After 04.10 12:00 UTC, the AR1 tracer fraction remains steady at a value of around 10% for the remainder of Cyclone B's lifespan. This steady contribution form AR1 is occurring during the merger of the first and the second AR (see section 4.2, figure 4.1 e and c). Some of the AR1 tracers is therefore present in the domain during the AR2 tracer initialization, leading to a duplicate tracer initialization, making them indistinguishable during the handover process to Cyclone C.

Precipitation from the AR tracers does not have the same distinct rapid decrease as the cyclone center tracers, Cy1 and Cy2 (Figure 5.22). The AR1 and AR2 tracers show a more continuous contribution throughout their respective cyclone's lifespan followed by a sharp drop (AR1 at 04.10.2016 1200 UTC and AR2 at 07.10.2016 00:00 UTC). The most remarkable feature captured here is from the AR1 tracer; it reaches a hiatus in precipitation contribution at 05.10.2016 00:00 UTC but 12 hours later it begins contributing again. This re-merging contribution persists for a period of about 65 hours with contributions of around 5%. Contributions from the AR1 tracer is even evident during the lifespan of Cyclone C. At 09.10.2016 00:00 both AR tracers reaches zero contribution almost simultaneously even though there are 60 hours of separation between each tracer initialization.

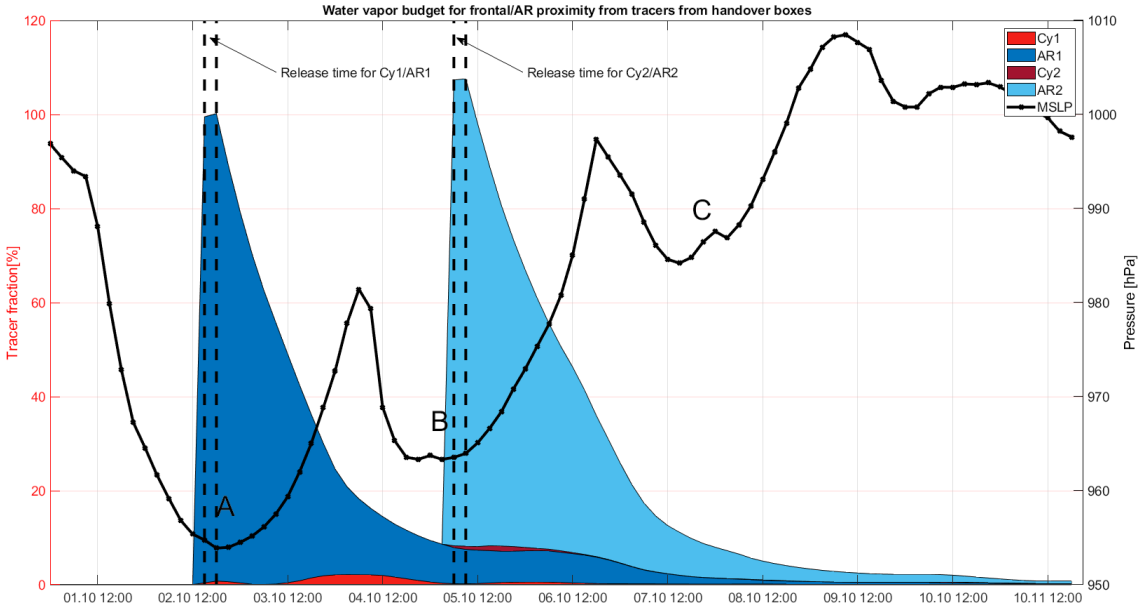

Figure 5.21: Water vapor budget for frontal/AR proximity(AR1/AR2 handover box, figure 3.2) for water vapor tracers. X-axis shows the time period 01-11.10 2020. Colored areas show tracer contributions, quantified as a fraction (%) compared to total TCWV in the respective box. Tracers from Cy1 (Red), AR1 (Blue), Cy2 (Dark red) and AR2(Light blue) are shown. The black solid and crossed line show the minimum MSLP in the Cy1/Cy2 box (hPa). Capital letters A, B and C denote cyclone periods

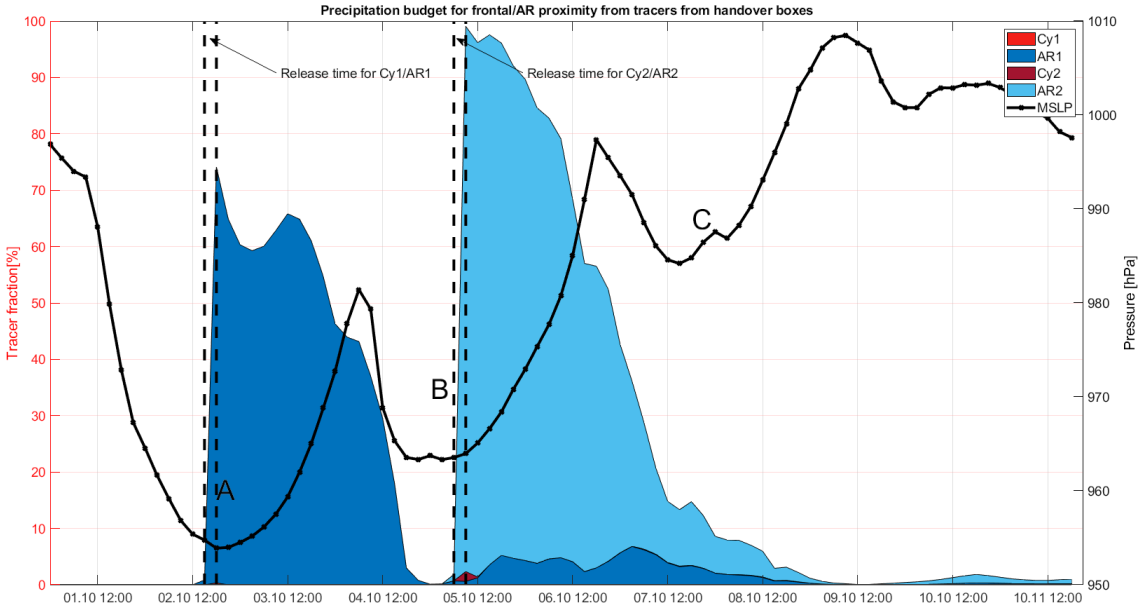

Figure 5.22: Same as Figure 5.21 but for precipitation

Chapter 6

Discussion

In this chapter, I will discuss the main results gathered in Chapter 5, in accordance to the literature. Furthermore, I will discuss the methods used and it's and limitations, as well as model validation. Finally, i discuss the implications of the results and give an outlook for future research.

Moisture origin in ARs and extratropical cyclones

Investigating moisture origin from extratropical cyclones during the time period 01-11.10.2016 reveal that the largest contribution to water vapor in proximity to the cyclones center is sea surface evaporation (50%) and advection of water vapor from the west (35-40%). This is in agreement with previous work conducted by Dacre et al. (2015) in that more local sea surface evaporation was the dominating contributor to the water vapor budget of extratropical cyclones. Moisture origin in water vapor associated the frontal structure or the AR of a cyclone also reveal that the largest contributor to water vapor is also sea surface evaporation (40%). However, the contribution from more remote sources i.e. the lateral boundaries are substantially different and shows a more even distribution. Adding the contributions from all the lateral boundaries give similar values as sea surface evaporation. The results from water vapor sources in ARs show similarities to the work done by Stohl et al. (2008) and Sodemann and Stohl (2013) in that more remote sources of water vapor is present in the AR. Combining these two viewpoints can give a larger picture in which water vapor sources are the largest contributor to the cyclone's water vapor, as a whole system including the frontal structure as well as close to its center. Vertical distribution of water vapor sources also found southern sources of water vapor residing at higher altitudes in the ARs which was also identified by Sodemann and Stohl (2013).

Vertical distributions of water vapor tracers in corresponding AR crossections investigated by the SAFIRE Falcon aircraft, (RF10, run010 07.10.2016 and RF13, run010 10.10.2016) show that the western, W and the eastern tracer, N/E have the greatest contribution to its respective western and eastern side of the AR. The southern tracer is residing at higher altitudes in the middle parts of the upper AR, however at much smaller

amounts with contribution of only 10% in regions of 0-2.5 g/kg. Similar results have been found by Sodemann and Stohl (2013) where they found more remote water vapor tracers residing at higher altitudes in ARs, compared to more local sources. The tracer contribution of the crossections of WCB outflows (RF11, run010 09.10.2016 and RF14, run010 11.10.2016) have predominantly contributions from the western tracer. On the 11.10.2016, contributions of 10% are found from both the S and N/E tracers in the eastern end of the crossection. Considering this is in the most moist part of the crossection, 10% is a considerable contribution.
Since the model run010 and the observations from the dropsondes are in overall agreement, especially in the ARs investigated, it is reasonable to assume that the vertical tracer distribution resemble the actual moisture distributions of the weather systems investigated by the SAFIRE Falcon aircraft during the NAWDEX field campaign.

Handover of water vapor between extratropical cyclones

The phenomenon of handover of moisture between extratropical cyclones have for the first time been identified and quantified. The hypothesis of sequential interaction between extra tropical cyclones in the form of an exchange of water vapor from ARs to cyclones was first put forward by Sodemann and Stohl (2013). This interaction have for the first time been quantified in here. The first event of the handover process is identified in Cyclone B, where water vapor tracers associated with the previous cyclone (Cyclone A) was identified. The water vapor was advected out of the area where Cyclone A was located in its later stages, and then later entered the airflow of the passing cyclone. Tracers from Cyclone A contribute 10% of the total moisture in Cyclone B. The second major event of the handover process is identified in Cyclone C. However, this incident has the strongest contribution from the AR associated with the previous cyclone (AR2). Here, the AR2 tracer contribute 10% to the total moisture in Cyclone C. The amount of water vapor handed over from the first cyclone to the second cyclone and from the AR (associated with the Cyclone B) to Cyclone C, is similar in fractional contributions. The most notable difference is how much of the water vapor that is handed over is used to generate precipitation; In the first handover event very small amounts of precipitation is attributed to the water vapor handed over (1%), but in the second event, upwards of 15 % of total precipitation is contributed from the water vapor handed over by the AR. This indicates that the AR is an important mechanism in the handover process and to effectively generate precipitation.
Handover of moisture is also identified from AR to AR, but since the domain is extended so far south, remnants of the first AR is present in the domain during the second tracer initialization. This means that tracer contributions from the tracer AR2 could in reality be from AR1, an prevents a clear interpretation. Tracer contributions to water vapor from AR1 found in the the frontal structure of the second cyclone and even in precipitation associated with the frontal structure during the early stages of the third cyclone.

Model validation

Comparison between the COSMO model run and the ERA-5 reanalysis data from ECMWF reveals large regional differences in bias and RMSE when looking at specific humidity, with alternating values of upwards of +/- 2 g/kg. However the bias calculated over the entire model domain show much lower values throughout the simulation period and no trend in over nor underrepresentation is identified (Section 5.1). This means that the the overall amount of moisture is well represented by the model but the locations of the moisture is not resolved. These results are similar to the previous study by Wick et al. (2013), where they evaluated the forecasts for ARs.

More qualitative model validation shows overall good agreement between the COSMO model and observations from dropsondes obtained from the SAFIRE Falcon aircraft during the NAWDEX field campaign (Section 5.2). By plotting vertical crossections of specific humidity and mixing ratio in areas of interest reveals that the over all vertical distribution of water vapor is well represented in both the coarse (run050) and the fine (run010) resolution model runs. Model run050 does not resolve the confined regions of the ARs, but run010 shows excellent agreement between the observations in both of the ARs investigated during the flights RF10 and RF13, and resolves both the vertical structure and the confined regions of the ARs.

Method limitations

There are some limitations in the method used here to quantify the handover of moisture between extratropical cyclones. In order to quantify the handover, water vapor tracers were released during a certain time period. Changing the duration of tracer release time could greatly alter the result in tracer contribution in the handover process. In this analysis the tracers were released in a 3 hour period and acts as a "snapshot" of the total moisture in the cyclone. This time period was chosen to make the water vapor tracers easily separable since the cyclones were generated in relatively short succession. To determine if releasing tracers for longer or shorter periods is the most optimal for quantifying the handover of moisture is not so straightforward. An additional model run were conducted where tracers were released during the majority of the respective cyclones lifespan. This can be found in the Appendix A.3.

Implications of results and outlook

To further investigate difference in moisture origin in water vapor associated with cyclone center proximity and the frontal structure or the AR by applying more elaborate measures of releasing water vapor tracers from sea surface evaporation could highlight the effects of local or more remote contributions of sea surface evaporation.

Sodemann and Stohl (2013) discuss briefly how forecasted precipitation amounts from NWP models could be affected if there is a sequential interaction between cyclones and their water vapor budgets. This sequential interaction has been identified here in the form of a handover of water vapor. The effects of this water vapor handover process in accordance to numerical weather prediction seem as a promising future study.

The frequency of occurrence of extratropical cyclones have increased in recent years (Pinto et al., 2014). With increasing frequency of extratropical cyclones also implies an increase of occurrence of ARs, and as a result of the Clausius Clapeyron relation, with a increasing temperature comes an increase of potential moisture content in these weather systems. This further implies that the handover process between extratropical cyclones could be increasing in magnitude in the same manner.

Chapter 7

Summary and conclusion

The main research aim of this thesis was to identify and quantify the handover of moisture between extratropical cyclones. Here, the atmospheric model with tracer capability, COSMO-tag was used to recreate the atmospheric conditions during the NAWDEX field campaign in the period 01-11.10.2016. The model was equipped with a water vapor tagging implementation, making it possible to identify from which sources water vapor is coming from, as well as to quantify the process of handover of moisture between extratropical cyclones. To showcase this process, two viewpoints have been presented to separate the water vapor associated with cyclone center proximity, and the frontal structure or the AR, associated with the respective cyclone. This helps to highlight the differences in moisture source contributions in the different weather systems.

To conclude, I will give a short summary of the main results discussed in this thesis:

- The phenomenon of handover of moisture between extratropical cyclones has been identified and quantified for the first time.
  - Contributions of around 10% of the total amount of water vapor in Cyclone B's center is attributed to water vapor handed over from Cyclone A.
  - Handover of moisture is also identified from AR to cyclone, with contributions of 10% from the second AR to Cyclone C
  - Amounts handed over from cyclone to cyclone and AR to cyclone have similar contributions in this case. However, the water vapor associated with the second AR contributes up to 15% in total precipitation during Cyclone C's lifespan. The Cy1 tracer from Cyclone A only contribute 1-2% of the precipitation associated with Cyclone B. The AR, thus seems to be an important mechanism to produce precipitation in the handover process.
- The largest moisture contribution to water vapor in proximity to the cyclone's center comes from sea surface evaporation and the western tracer, W, throughout the research period (Section 5.3, Table 5.1). Water vapor in the cyclone's frontal structure and the ARs also has the strongest contribution from sea

surface evaporation, but a stronger and more even contributions from the lateral boundary tracers W (western), N/E (Eastern) and S (Southern) (Section 5.3, Table 5.2).

- Vertical distribution of water vapor tracers in ARs show that more remote sources were residing at higher altitudes inside the AR. This corresponds well with the results from Sodemann and Stohl (2013).
- There is good agreement between mixing ratio and specific humidity, when comparing NAWDEX field campaign observations and model results. There is especially good agreement between the ARs resolved by dropsondes and the fine resolution model run (run010).
  - Because of the over all good agreement between model results and observations, and the previous statement on the vertical distribution of water vapor tracers, it is then reasonable to assume that the the vertical distribution of moisture sources resemble the actual distribution in the atmosphere during NAWDEX.

The results obtained here for the moisture origin in extratropical cyclones and ARs, as well as the handover of water vapor between extratropical cyclones, may be indicative of typical meteorological conditions in the North Atlantic fall. However, because these results only represent 3 separate extratropical cyclones in a relatively short period of 11 days, further analysis of similar conditions needs to be conducted for further insight in the process of handover of moisture.

Appendix A

Appendix A

A.1 Script for int2lm

Here the script for the prepossessing program int2lm script for the fine resolution (deg=0.1) is provided.

```
#!/bin/bash
#
# The INT2LM Job
#

#########################################################
# SETUP for the IAC Cluster

WDIR=int2lm_nawdex_deg010
WORK=/cluster/work/users/$USER
OUTDIR=$WORK/int2lm/output/${WDIR}/
EMAIL='Petter.Ekrem@student.uib.no'
QUEUE=normal
WALLTIME='2:0:0'

cd $WORK
mkdir $WORK/int2lm
mkdir $WORK/int2lm/output
mkdir $WORK/int2lm/input
mkdir $WORK/int2lm/input/$WDIR
mkdir $OUTDIR
RUNDIR=$WDIR
mkdir $RUNDIR
cd $RUNDIR

rm -f int2lm_job
```

```
# copy data files
cp -r /cluster/projects/nn9555k/data/int2lm/input/nawdex/cas201610*
...$WORK/int2lm/input/$WDIR
cp -r /cluster/projects/nn9555k/cosmo_tag/expar $WORK/int2lm
cp /cluster/projects/nn9555k/default_modules $WORK

#######################################################
# number of processors
#######################################################

NMULT=4  # number of cpus per node (change for new nodes!)
NPX=4
NPY=2
NPIO=0
NP1=`expr $NPX \* $NPY`
NP=`expr $NP1 + $NPIO`
N1=`expr $NP + $NMULT - 1`
NODES=`expr $N1 \/ $NMULT`

#######################################################
# prepare job skript
#######################################################

cat > int2lm_job  << EOF
#!/bin/bash
#-- Job settings:
#----------------

#### job name:
#SBATCH --account=nn9555k
#SBATCH --partition=${QUEUE}
#SBATCH --job-name=${WDIR}_int2lm_job
#SBATCH --mail-type=ALL
#SBATCH --mail-user=${EMAIL}
#/##SBATCH --output=${WORK}/int2lm/output

#### wall time limit
#SBATCH --time=$WALLTIME
#SBATCH --mem-per-cpu=4G

####SBATCH --ntasks=${NP} --ntasks-per-node=${NMULT} --cpus-per-task=10
#SBATCH --nodes=1 --ntasks=8 --cpus-per-task=2

echo "mother superior: \$(uname -n)"
#NSLOTS=\$(cat \$PBS_NODEFILE | wc -l)
#echo "running on \$NSLOTS cpus ..."
```

```
ulimit -s unlimited
ulimit -a

# load modules
source ${WORK}/default_modules

set -e

#--- Environment settings:
#-------------------------

MPIPROGINF='DETAIL'                     # program information
export MPIPROGINF                       # {NO|YES|DETAIL}
#
MPISUSPEND='ON'                         # select waiting method
export MPISUSPEND                       # {ON|OFF}={SUSPEND/RESUME|SPIN WAIT}
#
F_FTRACE='NO'                           # analysis list from compile opt. -ftrace
export F_FTRACE                         # {NO|YES|FMT0|FMT1|FMT2}
#
F_ERRCNT=0                              # stop execution after the first run time
                                        # error
export F_ERRCNT

#LD_LIBRARY_PATH="/opt/parastation/mpi2-intel/lib:${LD_LIBRARY_PATH}"
#export LD_LIBRARY_PATH
LIBDWD_FORCE_CONTROLWORDS=1
export LIBDWD_FORCE_CONTROLWORDS

#--- Loop over all files:
#------------------------

HINC=06
HSTOP=264
HADD=0
YDATE_START='2016100100'

rm -f YU* OUTPUT

while [ \${HADD} -le \${HSTOP} ]
do
YDATE_INI=\`/cluster/projects/nn9555k/bin/get_utc_date \${YDATE_START}
...\${HADD} 365\`

echo "running for " \${YDATE_INI}
```

```
#--- Prepare namelist file:
#-------------------------

cat > INPUT << end_input
 &CONTRL
   ydate_ini='\${YDATE_INI}',
   hstart=0.0, hstop=0.0, hincbound=0.0,
   nprocx=$NPX, nprocy=$NPY, lreorder=.FALSE.,
   yinput_model='CM', idbg_level=5,
   linitial=.TRUE., lboundaries=.FALSE.,
   ltime_mean=.TRUE., luvcor=.TRUE.,
   lfilter_pp=.FALSE., lbalance_pp=.FALSE., norder_filter=5,
   lfilter_oro=.TRUE., eps_filter=0.1,
   ilow_pass_oro=1, ilow_pass_xso=0, rxso_mask=0.0,
   lprog_qi=.TRUE., lpost_0006=.TRUE.,
   lmulti_layer_in=.TRUE., lmulti_layer_lm=.TRUE., l_smi=.FALSE.,
   lsso=.TRUE., lforest=.TRUE., lt_cl_corr=.TRUE., luse_t_skin=.TRUE.,
   itype_w_so_rel=3,
   itype_t_cl=1,
   itype_rootdp=0,
   itype_ndvi=0,
   lprog_qr_qs=.FALSE., lprog_rho_snow=.FALSE.,
   luvcor=.TRUE., lvertwind_ini=.TRUE., lvertwind_bd=.TRUE.,
   liso=.FALSE.,
 /
&GRID_IN
   ie_in_tot=1440,
   je_in_tot=361,
   ke_in_tot=137,
   pollon_in=180.0, pollat_in=90.0,
   dlon_in=0.25,
   dlat_in=0.25,
   startlon_in_tot=-180.0,
   startlat_in_tot=0.0,
   endlon_in_tot=179.75,
   endlat_in_tot=90.0,
   pcontrol_fi=30000.0,
   ke_soil_in=3,
   czml_soil_in=0.035,0.175,0.64,1.775,
 /
 &LMGRID
   ielm_tot=352, jelm_tot=482, kelm_tot=40,
   pollon=143.0, pollat=45.0,
   dlon=0.1, dlat=0.1,
   startlon_tot=-9.6, startlat_tot=-9.6,
   ke_soil_lm=7,
```

```
  czml_soil_lm=0.005, 0.02, 0.06, 0.18, 0.54, 1.62, 4.86, 14.58,
 /
 &DATABASE
 /
 &DATA
  ylmext_cat='$WORK/int2lm/expar/',
  ylmext_lfn='COSMO_NAWDEX_360x490.nc',
  ie_ext=360, je_ext=490,
  yinext_cat='$WORK/int2lm/input/$WDIR/',
  yinext_lfn='cas\${YDATE_INI}.nc',
  yin_cat='$WORK/int2lm/input/$WDIR/',
  ylm_cat='$OUTDIR',
  yinput_type='analysis'
  nprocess_ini=131, nprocess_bd=132,
  yinext_form_read='ncdf', yin_form_read='ncdf',
  ylmext_form_read='ncdf'
 /
 &PRICTR
  igp_tot = 36, 40, 48, 44, 48, 85, 77
  jgp_tot = 30, 94, 38, 26, 26, 96, 12
  lchkin=.TRUE., lchkout=.TRUE.,
 /
end_input

#-- Start the run:
#-------------------

rm -f YUCHKDAT YUTIMING YUDEBUG OUTPUT
#mpiexec -np $NP /cluster/projects/nn9555k/progs/int2lm-iso-17O-2.0/int2lm
mpiexec -launcher slurm -n 8  /cluster/projects/nn9555k/progs/
...int2lm-iso-17O-2.0/int2lm
rm INPUT

HADD=\`expr \${HADD} + \${HINC}\`

done

mkdir /nird/projects/nird/NS9054K/int2lm/output/$WDIR
rsync -r $OUTDIR/* /nird/projects/nird/NS9054K/int2lm/output/$WDIR

#-- Notification that job is finished:
#--------------------------------------

mailx -s "Job $WDIR finished!" $EMAIL <<EOF_mail
Model run $WDIR finished at \`date\` on \`uname -n\`
Last output file produced: \`ls -lrt $OUTDIR | tail -1\`
```

```
EOF_mail

cp slurm* $OUTDIR

EOF

#####################################################
# launch the job
#####################################################

echo "Submitting int2lm_job:"
echo "      -on $QUEUE"
echo "      -with $NODES nodes"
echo "      -for a walltime of $WALLTIME"

sbatch int2lm_job

# fin
```

A.2 Script for COSMO run 010

Here the script for the fine resolution (deg=0.1) COSMO model run010 is provided.

```
#!/bin/bash
#
# The COSMO Job
#

#####################################################
# SETUP for the IAC Cluster

WDIR=cosmo_tag_nawdex_deg010_9box_run04
WORK=/cluster/work/users/$USER
OUTDIR=$WORK/cosmo/output/${WDIR}/
RESTART=$WORK/cosmo/restart/${WDIR}/
EMAIL='Petter.Ekrem@student.uib.no'
QUEUE=normal
WALLTIME='24:00:00'

#cd $SCRATCH
cd $WORK
mkdir $WORK/cosmo
mkdir $WORK/cosmo/output
mkdir $WORK/cosmo/input
```

```
mkdir $WORK/cosmo/input/$WDIR
mkdir $WORK/cosmo/restart
mkdir $OUTDIR
RUNDIR=$WDIR
mkdir $RUNDIR
mkdir $RESTART
cd $RUNDIR

rm -f make_cosmo_job
rm -f INPUT_ORG INPUT_IO INPUT_DYN INPUT_DIA INPUT_PHY
rm -f INPUT_INI INPUT_ASS INPUT_TAG
rm -f YU* OUTPUT*

# copy data files
cp /cluster/projects/nn9555k/data/int2lm/int2lm_nawdex_deg010/laf201610*
...$WORK/cosmo/input/$WDIR
cp /cluster/projects/nn9555k/default_modules $WORK

#####################################################
# number of processors
#####################################################

NMULT=4  # number of cpus per node (change for new nodes!)
NPX=4
NPY=4
NPIO=1
NP1=`expr $NPX \* $NPY`
NP=`expr $NP1 + $NPIO`
N1=`expr $NP + $NMULT - 1`
NODES=`expr $N1 \/ $NMULT`
echo $NODES $NMULT

#####################################################
# prepare job skript
#####################################################

cat > make_cosmo_job  << EOF
#!/bin/bash
#-- Job settings:
#----------------

#### job name:
#SBATCH --account=nn9555k
#SBATCH --partition=${QUEUE}
#SBATCH --job-name=${WDIR}_job
#SBATCH --mail-type=ALL
```

```
#SBATCH --mail-user=${EMAIL}
#/##SBATCH --output=${WORK}/int2lm/output

#### wall time limit
#SBATCH --time=$WALLTIME
#SBATCH --mem-per-cpu=4G

####SBATCH --ntasks=${NP} --ntasks-per-node=${NMULT} --cpus-per-task=10
#SBATCH --nodes=1 --ntasks=17 --cpus-per-task=1

ulimit -s unlimited
ulimit -a

# load modules
source ${WORK}/default_modules

set -e

#--- Environment settings:
#----------------------------

MPIPROGINF='DETAIL'                    # program information
export MPIPROGINF                      # {NO|YES|DETAIL}
#
MPISUSPEND='ON'                        # select waiting method
export MPISUSPEND                      # {ON|OFF}={SUSPEND/RESUME|SPIN WAIT}
#
F_FTRACE='NO'                          # analysis list from compile opt. -ftrace
export F_FTRACE                        # {NO|YES|FMT0|FMT1|FMT2}
#
F_ERRCNT=0                             # stop execution after the first run time
                                       # error
export F_ERRCNT

#LD_LIBRARY_PATH="${LD_LIBRARY_PATH}"
#export LD_LIBRARY_PATH
LIBDWD_FORCE_CONTROLWORDS=1
export LIBDWD_FORCE_CONTROLWORDS

#--- Prepare namelist files:
#----------------------------

cat > INPUT_ORG << end_input_org
 &LMGRID
   startlon_tot=-9.6, startlat_tot=-9.6,
   pollon=143.0,          pollat=45.0,
```

```
  dlon=0.1,           dlat=0.1,
  ie_tot=352,          je_tot=482,          ke_tot=40,
 /

 &RUNCTL
  ydate_ini='2016100100',
  ydate_bd='2016100100',
  dt=120.0,
  hstart=0.0,    hstop=264.0,
  idbg_level=1000,
  lreproduce=.TRUE., luseobs=.FALSE.,
  lphys=.TRUE., ldiagnos=.TRUE., ldfi=.FALSE.,
  luse_rttov=.FALSE.,
  nprocx= $NPX, nprocy= $NPY, nprocio=$NPIO,
  nboundlines=4, lreorder=.FALSE.,
  ldatatypes=.FALSE.,
  ncomm_type=1, ltag=.TRUE.,
 /
 &TUNING
  clc_diag=0.5, rat_lam=1.0, rat_can=1.0,
  c_soil=1.0, v0snow=25.0,
  wichfakt=0.0, crsmin=150., qc0=0.0, qi0=0.0,
 /
end_input_org

cat > INPUT_IO  << end_input_io
 &IOCTL
  ngribout=1, lasync_io=.FALSE.,
  lbdclim=.TRUE.,
 /
 &DATABASE
 /
 &GRIBIN
  ydirini='/cluster/work/users/$USER/cosmo/input/$WDIR/',
  lchkini=.TRUE.,
  lana_qi=.FALSE., lana_qr_qs=.FALSE., lana_rho_snow=.FALSE.,
  ydirbd='/cluster/work/users/$USER/cosmo/input/$WDIR/',
  hincbound=6.0,
  lchkbd=.TRUE.,
  llb_qi=.FALSE., llb_qr_qs=.FALSE.,
  lbdana=.TRUE.,
  lan_t_so0=.TRUE., lan_t_cl=.TRUE., lan_w_cl=.TRUE.,
  lan_vio3=.TRUE., lan_hmo3=.TRUE., lan_plcov=.TRUE., lan_lai=.TRUE.,
  lan_rootdp=.TRUE., lan_t_snow=.TRUE., lan_w_i=.TRUE., lan_w_snow=.TRUE.,
  lan_rho_snow=.TRUE.,
 /
```

```
 &GRIBOUT
  ysystem='file',
  yform_write='ncdf',
  hcomb= 0.,264.0,3.0,
  l_p_filter=.TRUE.,
  l_z_filter=.TRUE.,
  ytunit='d',
  yvarml='TQVTAG1', 'TQVTAG2', 'TQVTAG3', 'TQVTAG4', 'TQVTAG5', 'TQVTAG6',
  'TQVTAG7', 'TQVTAG8', 'TQVTAG9', 'TQVTAG10', 'QVTAG1', 'QVTAG2',
  'QVTAG3', 'QVTAG4', 'QVTAG5', 'QVTAG6', 'QVTAG7', 'QVTAG8', 'QVTAG9',
  'QVTAG10', 'R_TAG_G1', 'R_TAG_G2', 'R_TAG_G3', 'R_TAG_G4', 'R_TAG_G5',
  'R_TAG_G6', 'R_TAG_G7', 'R_TAG_G8', 'R_TAG_G9', 'R_TAG_G10', 'U',
  'V', 'W', 'P', 'T', 'T_S', 'QV', 'QC', 'QI', 'QR', 'QS', 'PS', 'PMSL',
  'RAIN_GSP', 'SNOW_GSP', 'RAIN_CON', 'SNOW_CON', 'TOT_PREC', 'AEVAP_S',
  'HPBL', 'EVAPTOT', 'BSEVAP', 'IEVAP', 'PTEVAP', 'SNOEVAP', 'W_SO', 'W_SNOW'
  'ASHFL_S', 'T_2M', 'U_10M', 'V_10M',
  yvarpl='default',
  yvarzl='default',
  yvarsl='default',
  lcheck=.TRUE.,
  lwrite_const=.TRUE.,
  ydir='$OUTDIR',
 /
end_input_io

cat > INPUT_DYN << end_input_dyn
 &DYNCTL
  l2tls=.TRUE.,
  irunge_kutta=2,
  irk_order=3,
  iadv_order=5,
  y_scalar_advect='Bott4',
  y_vert_adv_dyn='impl2',
  ieva_order=3,
  ldiabf_lh=.TRUE.,
  lsemi_imp=.FALSE., lcond=.TRUE.,
  lspubc=.TRUE., lexpl_lbc=.TRUE., ldyn_bbc=.TRUE.,
  betasw=0.4, xkd=0.1, epsass=0.15,
  lhordiff=.TRUE., itype_hdiff=2,
  hd_corr_u_bd=0.25, hd_corr_u_in=0.25,
  hd_corr_t_bd=0.0, hd_corr_t_in=0.0,
  hd_corr_q_bd=0.0,  hd_corr_q_in=0.0,
  hd_corr_p_bd=0.0,  hd_corr_p_in=0.0,
  hd_dhmax=250.0, itype_bbc_w=2,
 /
end_input_dyn
```

```
cat > INPUT_PHY << end_input_phy
 &PHYCTL
     lgsp=.TRUE., itype_gscp=3, lprogprec=.TRUE., ldiniprec=.FALSE.,
                  ltrans_prec=.TRUE.,
     lrad=.TRUE., hincrad=1.0, nradcoarse=1, lradf_avg=.FALSE.,
     ltur=.TRUE., itype_turb=3, ninctura=1, imode_turb=1,
                  itype_tran=2, imode_tran=1,
                  lexpcor=.FALSE., ltmpcor=.FALSE., lprfcor=.FALSE.,
                  lnonloc=.FALSE., lcpfluc=.FALSE., limpltkediff=.TRUE.,
                  itype_wcld=2, icldm_rad=4, icldm_turb=2, icldm_tran=0,
                  itype_synd=2,
     lsoil=.TRUE., itype_evsl=2, itype_trvg=2,
                   lmulti_layer=.TRUE., lmelt=.TRUE., lmelt_var=.TRUE.,
                   ke_soil=7,
                   czml_soil = 0.005, 0.02, 0.06, 0.18, 0.54, 1.62, 4.86,
                   ...14.58,
     lconv=.TRUE., lcape=.FALSE., nincconv=4,
     lforest=.TRUE., llake=.FALSE., lseaice=.FALSE., lsso=.TRUE.
 /
end_input_phy

cat > INPUT_DIA << end_input_dia
 &DIACTL
   n0gp=0,       hincgp=1.0,
   n0meanval=0, nincmeanval=1,
   lgplong=.FALSE., lgpshort=.TRUE., lgpspec=.FALSE.,
 /
end_input_dia

cat > INPUT_INI << end_input_ini
 &INICTL
   ndfi=2, nfilt=1,
   tspan=3600.0, taus=3600.0,
   dtbak=40.0, dtfwd=40.0,
 /
end_input_ini

cat > INPUT_ASS << end_input_ass
 &NUDGING
   lnudge=.FALSE.,
 /
end_input_ass

cat > INPUT_TAG << end_input_tag
 &TAGCTL
```

```
  ltagbox=.TRUE.,
  ltagstat=.FALSE.,
  ltagslab=.FALSE.,
  ltagreg=.FALSE.,
  itag=9,
  islab=0,
  ibox=10,
  istat=1,
  levapflux_tag=.TRUE.,
/
&TAGBOX
  use_box=.TRUE.,
  xstart_l=5,
  ystart_l=5,
  zstart_l=1,
  xend_l=348,
  yend_l=478,
  zend_l=40,
  tstart_l=10600,
  tend_l=11200,
  box_id_l=1,
  rayl_tag_l=.TRUE.,
  relax_tag_l=.FALSE.,
/
&TAGBOX
  use_box=.TRUE.,
  xstart_l=349,
  ystart_l=5,
  zstart_l=1,
  xend_l=352,
  yend_l=482,
  zend_l=40,
  tstart_l=10600,
  tend_l=950400,
  box_id_l=2,
  rayl_tag_l=.TRUE.,
  relax_tag_l=.TRUE.,
/
&TAGBOX
  use_box=.TRUE.,
  xstart_l=5,
  ystart_l=479,
  zstart_l=1,
  xend_l=348,
  yend_l=482,
  zend_l=40,
```

```
  tstart_l=10600,
  tend_l=950400,
  box_id_l=2,
  rayl_tag_l=.TRUE.,
  relax_tag_l=.TRUE.,
/
&TAGBOX
  use_box=.TRUE.,
  xstart_l=1,
  ystart_l=1,
  zstart_l=1,
  xend_l=4,
  yend_l=482,
  zend_l=40,
  tstart_l=10600,
  tend_l=950400,
  box_id_l=3,
  rayl_tag_l=.TRUE.,
  relax_tag_l=.TRUE.,
/
&TAGBOX
  use_box=.TRUE.,
  xstart_l=5,
  ystart_l=1,
  zstart_l=1,
  xend_l=352,
  yend_l=4,
  zend_l=40,
  tstart_l=10600,
  tend_l=950400,
  box_id_l=4,
  rayl_tag_l=.TRUE.,
  relax_tag_l=.TRUE.,
/
&TAGBOX
  use_box=.TRUE.,
  xstart_l=55,
  ystart_l=185,
  zstart_l=1,
  xend_l=180,
  yend_l=325,
  zend_l=40,
  tstart_l=151200,
  tend_l=162000,
  box_id_l=5,
  rayl_tag_l=.TRUE.,
```

```
  relax_tag_l=.FALSE.,
/
&TAGBOX
  use_box=.TRUE.,
  xstart_l=181,
  ystart_l=10,
  zstart_l=1,
  xend_l=275,
  yend_l=325,
  zend_l=40,
  tstart_l=151200,
  tend_l=162000,
  box_id_l=6,
  rayl_tag_l=.TRUE.,
  relax_tag_l=.FALSE.,
/
&TAGBOX
  use_box=.TRUE.,
  xstart_l=55,
  ystart_l=185,
  zstart_l=1,
  xend_l=180,
  yend_l=325,
  zend_l=40,
  tstart_l=378000,
  tend_l=388800,
  box_id_l=7,
  rayl_tag_l=.TRUE.,
  relax_tag_l=.FALSE.,
/
&TAGBOX
  use_box=.TRUE.,
  xstart_l=181,
  ystart_l=10,
  zstart_l=1,
  xend_l=275,
  yend_l=325,
  zend_l=40,
  tstart_l=378000,
  tend_l=388800,
  box_id_l=8,
  rayl_tag_l=.TRUE.,
  relax_tag_l=.FALSE.,
/
&TAGBOX
  use_box=.TRUE.,
```

```
  xstart_l=5,
  ystart_l=5,
  zstart_l=40,
  xend_l=348,
  yend_l=478,
  zend_l=40,
  tstart_l=10600,
  tend_l=950400,
  box_id_l=9,
  rayl_tag_l=.TRUE.,
  relax_tag_l=.FALSE.,
 /
 &TAGSLAB
  use_slab=.TRUE.,
  slab_id_l=9,
  slabfile_l='/cluster/projects/nn9555k/data/slab/landmask_deg010.slb',
 /
 &TAGSLAB
  use_slab=.TRUE.,
  slab_id_l=10,
  slabfile_l='/cluster/projects/nn9555k/data/slab/seamask_deg010.slb',
 /
 &TAGSTAT
  use_stat=.FALSE.,
  xstart_s_l=98,
  ystart_s_l=62,
  zstart_s_l=1, xend_s_l=105,
  yend_s_l=75,
  zend_s_l=40,
  tstart_s_l=0,
  tend_s_l=3974400,
  statfile_l='TAG_STAT_NNOR'
 /
end_input_tag

#-- Start the run:
#-------------------

mpiexec -launcher slurm -n 17 /cluster/projects/nn9555k/progs/cosmo_tagging/
...cosmo_tag_paropt
#mpiexec -np $NP /cluster/projects/nn9555k/progs/cosmo_tagging/
...cosmo_tag_paropt
rm -f INPUT_*

#-- Notification that job is finished:
#-----------------------------------
```

```
mailx -s "Job $WDIR finished!" $EMAIL <<EOF_mail
Model run $WDIR finished at \`date\` on \`uname -n\`
Last output file produced: \`ls -lrt $OUTDIR | tail -1\`
EOF_mail

# copy results to nird for storage
mkdir /nird/projects/nird/NS9054K/cosmo_tag/output/$WDIR
rsync -rv $WORK/cosmo/output/${WDIR}/* /nird/projects/nird/NS9054K/cosmo/
...output/$WDIR

EOF

# RESTART OPTIONS from INPUT_IO
# nhour_restart=120,240,120,
# ydir_restart='${RESTART}',
# ytunit_restart='d',

#####################################################
# launch the job
#####################################################

echo "Submitting make_cosmo_job:"
echo "      -on $QUEUE"
echo "      -with $NODES nodes"
echo "      -for a walltime of $WALLTIME"

sbatch make_cosmo_job
```

A.3 Quantifying handover with longer tracer initialization

In this section I present the results from investigating the handover process but with longer tracer initialization time. Here the water vapor tracers were released throughout the time period of the lifespan of the respective cyclone, compared to the 3-hour period used for the analysis in section 5.5. The results here indicate that the resolved events of handover of water vapor is the same are the same events identified previously in the study, however the amounts are amplified because of the longer tracer initialization time. All tracers have a longer lifetime in the domain and secondary handover process can even be identified where tracers remain through multiple cyclones lifespan. One notable difference between the longer tracer initialization time model run is the contribution in precipitation from the tracer Cy1 during the second cyclones lifespan. Here Cy1 contributes upwards if 15% throughout the second cyclones lifespan (Figure A.2.

There is one major caveat of releasing water vapor tracers during longer time periods; It is difficult to separate to which cyclone the water vapor is associated with since the cyclones are being generated in relatively short time periods.

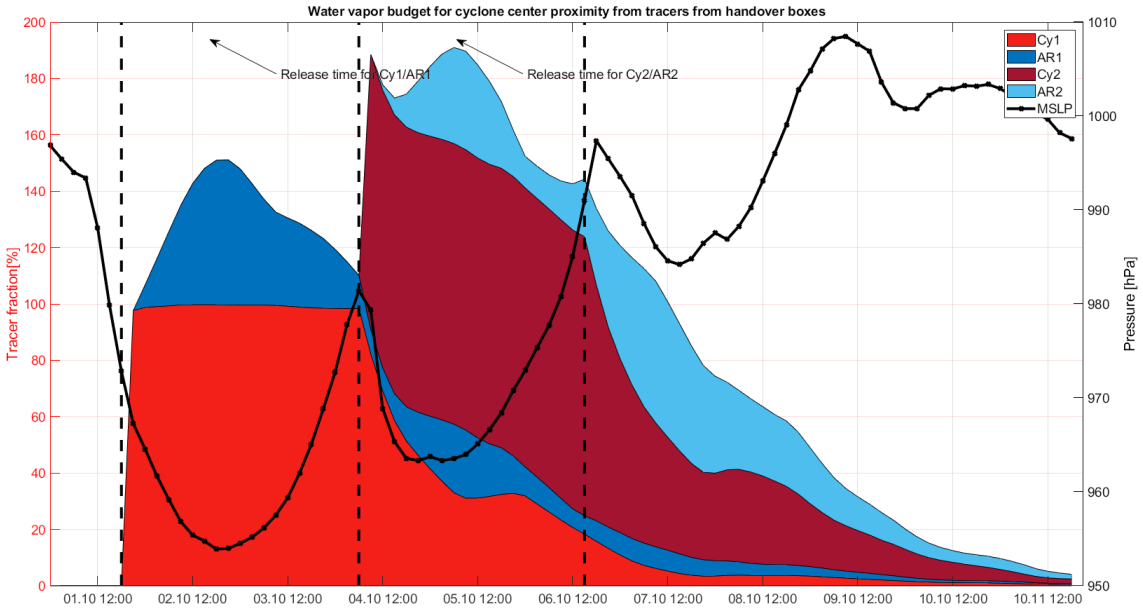

Figure A.1: Water vapor budget for cyclone center proximity(Cy1/Cy2 handover box, figure 3.2) for water vapor tracers. X-axis shows the time period 01-11.10 2020. Colored areas show tracer fraction (Left y-axis [%]) compared to total TCWV in the respective box. Tracers from Cy1 (Red),AR1 (Blue), Cy2 (Dark red) and AR2(Light blue) are shown. The black solid and crossed line show the minimum MSLP in the Cy1/Cy2 box (Right y-axis[hPa])

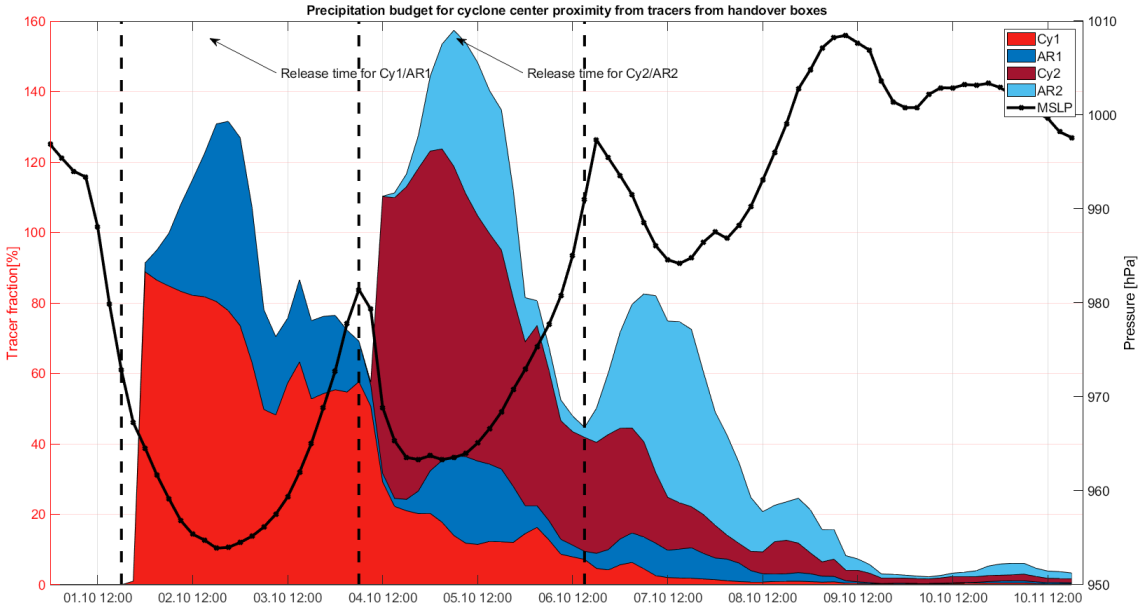

Figure A.2: Precipitation budget for cyclone center proximity(Cy1/Cy2 handover box, figure 3.2) for water vapor tracers. X-axis shows the time period 01-11.10 2020. Colored areas show tracer fraction (Left y-axis [%]) compared to total TCWV in the respective box. Tracers from Cy1 (Red),AR1 (Blue), Cy2 (Dark red) and AR2(Light blue) are shown. The black solid and crossed line show the minimum MSLP in the Cy1/Cy2 box (Right y-axis[hPa])

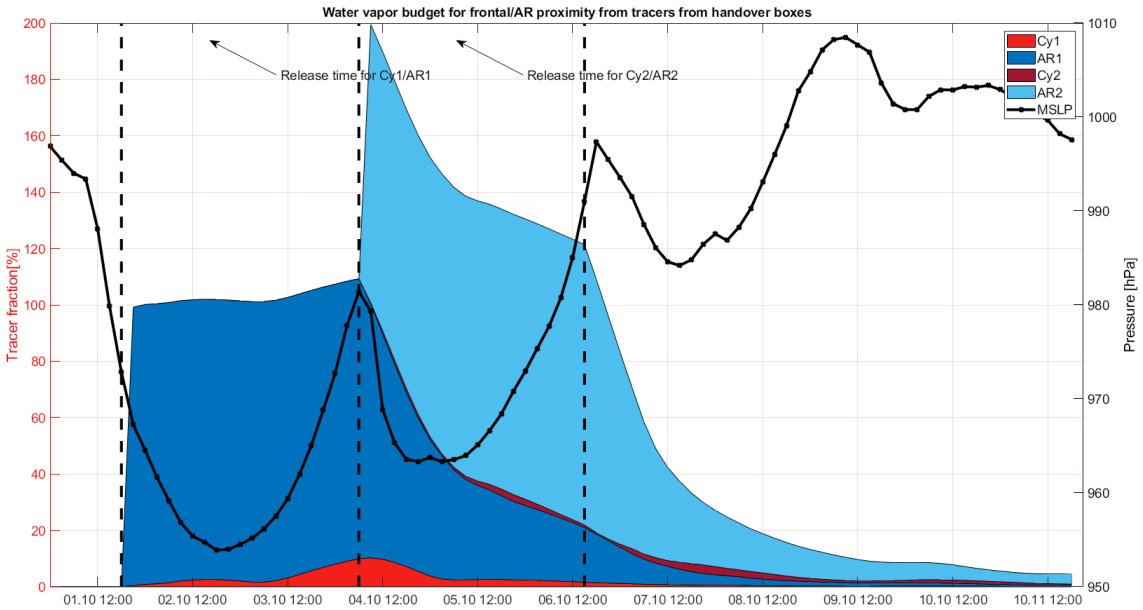

Figure A.3: Water vapor budget for frontal/AR proximity(AR1/AR2 handover box, figure 3.2) for water vapor tracers. X-axis shows the time period 01-11.10 2020. Colored areas show tracer fraction (Left y-axis [%]) compared to total TCWV in the respective box. Tracers from Cy1 (Red),AR1 (Blue), Cy2 (Dark red) and AR2(Light blue) are shown. The black solid and crossed line show the minimum MSLP in the Cy1/Cy2 box (Right y-axis[hPa])

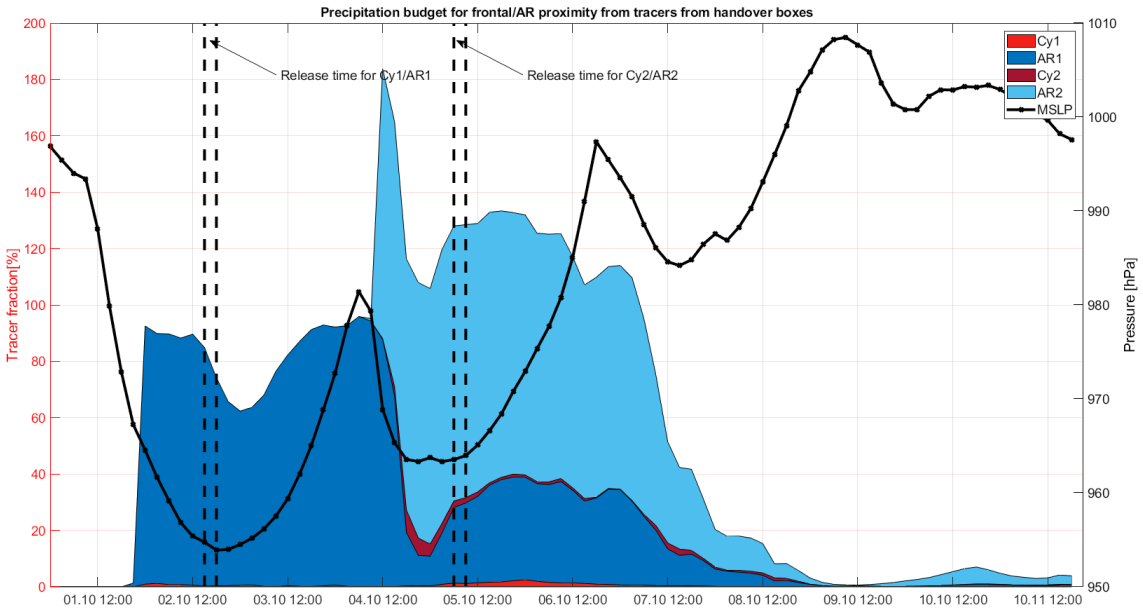

Figure A.4: Precipitation budget for frontal/AR proximity(AR1/AR2 handover box, figure 3.2) for water vapor tracers. X-axis shows the time period 01-11.10 2020. Colored areas show tracer fraction (Left y-axis [%]) compared to total TCWV in the respective box. Tracers from Cy1 (Red),AR1 (Blue), Cy2 (Dark red) and AR2(Light blue) are shown. The black solid and crossed line show the minimum MSLP in the Cy1/Cy2 box (Right y-axis[hPa])

A.4 Vertical distribution of water vapor tracers, including sea surface evaporation

The vertical distribution of water vapor tracers from sea surface evaporation have a more uniform distribution compared to the tracer from lateral boundaries. The greatest contribution is closer to the surface and decreases with height (Figure A.5 b), c), and d)). One exception is the AR during 07.10.2016. Here the SEvap tracer is contribution with values of above 50% throughout major parts of the AR, notably even at higher altitudes (600hPa) (Figure A.5 a).

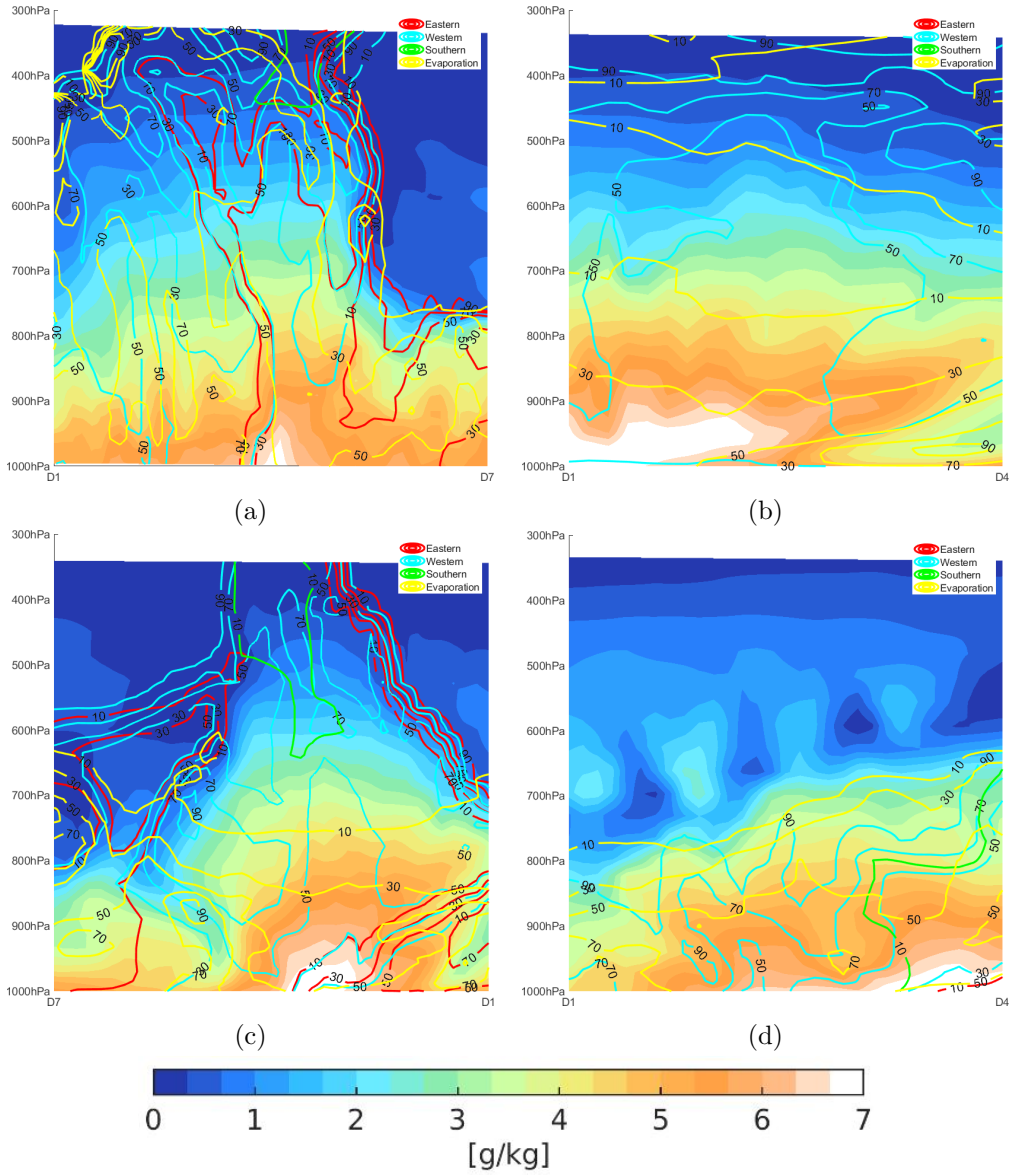

Figure A.5: Vertical distribution of water vapor tracers (contours; fraction (%)) and crossection of specific humidity from run010 (shading; g/kg). Tracer contributions from N/E (red), W (Cyan), S (Green) and SEvap (yellow) are shown. Crossections are for the dates corresponding to the dates of flights a) RF10, b) RF11, c) RF13 and d) RF14

References

J. M. Cordeira, F. Martin Ralph, and B. J. Moore. The development and evolution of two atmospheric rivers in proximity to western north pacific tropical cyclones in october 2010. *Monthly Weather Review*, 141(12):4234–4255, 2013. ISSN 15200493. doi: 10.1175/MWR-D-13-00019.1.

H. F. Dacre, P. A. Clark, O. Martinez-Alvarado, M. A. Stringer, and D. A. Lavers. How do atmospheric rivers form? *Bulletin of the American Meteorological Society*, 96(8):1243–1255, 2015. ISSN 00030007. doi: 10.1175/BAMS-D-14-00031.1.

Doms, G. Doms, and C. Schraff. Consortium for Small-Scale Modelling A Description of the Nonhydrostatic Regional COSMO-Model Part I : Dynamics and Numerics . (October), 2013.

EPATAN. EPATAN Flight Report 21.10.2016. 2016.

L. Gimeno, R. Nieto, M. Vázquez, and D. A. Lavers. Atmospheric rivers: A mini-review, mar 2014. ISSN 22966463.

W. Harrold. Baroclinic Disturbances. (lc):232–251, 1972.

M. K. Hawcroft, L. C. Shaffrey, K. I. Hodges, and H. F. Dacre. How much Northern Hemisphere precipitation is associated with extratropical cyclones? *Geophysical Research Letters*, 39(24), 2012. ISSN 19448007. doi: 10.1029/2012GL053866.

H. Hersbach, B. Bell, P. Berrisford, S. Hirahara, A. Horányi, J. Muñoz-Sabater, J. Nicolas, C. Peubey, R. Radu, D. Schepers, A. Simmons, C. Soci, S. Abdalla, X. Abellan, G. Balsamo, P. Bechtold, G. Biavati, J. Bidlot, M. Bonavita, G. De Chiara, P. Dahlgren, D. Dee, M. Diamantakis, R. Dragani, J. Flemming, R. Forbes, M. Fuentes, A. Geer, L. Haimberger, S. Healy, R. J. Hogan, E. Hólm, M. Janisková, S. Keeley, P. Laloyaux, P. Lopez, C. Lupu, G. Radnoti, P. de Rosnay, I. Rozum, F. Vamborg, S. Villaume, and J. N. Thépaut. The ERA5 global reanalysis. *Quarterly Journal of the Royal Meteorological Society*, 146(730): 1999–2049, 2020. ISSN 1477870X. doi: 10.1002/qj.3803.

P. J. Neiman, F. M. Ralph, G. A. Wick, J. D. Lundquist, and M. D. Dettinger. Meteorological characteristics and overland precipitation impacts of atmospheric rivers affecting the West coast of North America based on eight years of SSM/I satellite observations. *Journal of Hydrometeorology*, 9(1):22–47, 2008. ISSN 1525755X. doi: 10.1175/2007JHM855.1.

R. E. Newell, N. E. Newell, Y. Zhu, and S. Coutney. Tropospheric rivers? - A PILOT STUDY. pages 2401– –2404, 1992.

J. G. Pinto, I. Gómara, G. Masato, H. F. Dacre, T. Woollings, and R. Caballero. Journal of Geophysical Research : Atmospheres. *Journal of Geophysical Research*, pages 704–719, 2014. doi: 10.1002/2014JD022305.Received.

A. Schäfler, G. Craig, H. Wernli, P. Arbogast, J. D. Doyle, R. McTaggart-Cowan, J. Methven, G. Rivière, F. Ament, M. Boettcher, M. Bramberger, Q. Cazenave, R. Cotton, S. Crewell, J. Delanoë, A. Dörnbrack, A. Ehrlich, F. Ewald, A. Fix, C. M. Grams, S. L. Gray, H. Grob, S. Groß, M. Hagen, B. Harvey, L. Hirsch, M. Jacob, T. Kölling, H. Konow, C. Lemmerz, O. Lux, L. Magnusson, B. Mayer, M. Mech, R. Moore, J. Pelon, J. Quinting, S. Rahm, M. Rapp, M. Rautenhaus, O. Reitebuch, C. A. Reynolds, H. Sodemann, T. Spengler, G. Vaughan, M. Wendisch, M. Wirth, B. Witschas, K. Wolf, and T. Zinner. The North Atlantic Waveguide and Downstream Impact Experiment. *Bulletin of the American Meteorological Society*, (August):BAMS–D–17–0003.1, 2018. ISSN 00030007. doi: 10.1175/BAMS-D-17-0003.1.

H. Sodemann and A. Stohl. Moisture Origin and Meridional Transport in Atmospheric Rivers and Their Association with Multiple Cyclones*. *Monthly Weather Review*, 141(8):2850–2868, 2013. ISSN 0027-0644. doi: 10.1175/MWR-D-12-00256.1.

A. Stohl, C. Forster, and H. Sodemann. Remote sources of water vapor forming precipitation on the Norwegian west coast at 60°N - A tale of hurricanes and an atmospheric river. *Journal of Geophysical Research Atmospheres*, 113(5):1–13, 2008. ISSN 01480227. doi: 10.1029/2007JD009006.

C. D. Thorncroft, B. J. Hoskins, and M. E. McIntyre. Two paradigms of baroclinic-wave life-cycle behaviour. *Quarterly Journal of the Royal Meteorological Society*, 119(509):17–55, 1993. ISSN 1477870X. doi: 10.1002/qj.49711950903.

Vaisala. Vaisala Dropsonde RD94 Manual.

T. T. Warner. *Numerical weather and climate prediction*. Cambridge University Press, 2011. ISBN 9780511763243.

G. A. Wick, P. J. Neiman, F. M. Ralph, and T. M. Hamill. Evaluation of forecasts of the water vapor signature of atmospheric rivers in operational numerical weather prediction models. *Weather and Forecasting*, 28(6):1337–1352, dec 2013. ISSN 08828156. doi: 10.1175/WAF-D-13-00025.1.

A. Winschall, S. Pfahl, H. Sodemann, and H. Wernli. Comparison of Eulerian and Lagrangian moisture source diagnostics – the flood event in eastern Europe in May 2010. pages 6605–6619, 2014. doi: 10.5194/acp-14-6605-2014.

Y. Zhu and R. E. Newell. A Proposed Algorithm for Moisture Fluxes from Atmospheric Rivers. *Monthly Weather Review*, 126(3):725–735, 1998. ISSN 0027-0644. doi: 10.1175/1520-0493(1998)126¡0725:APAFMF¿2.0.CO;2.